Energy Conversion and Management 344 (2025) 120269

Contents lists available at ScienceDirect

Energy Conversion and Management

journal homepage: www.elsevier.com/locate/enconman

Optimal design of CO_2 Carnot battery technology for long duration energy storage

Simone Girelli, Dario Alfani *, Ettore Morosini, Marco Astolfi

Politecnico di Milano, Dipartimento di Energia, Via Lambruschini 4, 20156 Milano, Italy

ARTICLE INFO

Keywords:
CO_2 Carnot battery
Long duration energy storage
Sensible solid energy storage
Pumped thermal energy storage
Thermodynamic analysis
Round trip efficiency

ABSTRACT

CO_2-based Carnot battery systems are a promising solution for large scale, long duration energy storage, as they combine high round-trip efficiency with the absence of geological constraints, also enabling the storage of both hot and cold thermal energy. In this work, the optimal design criteria for a CO_2-based Carnot battery are discussed, focusing on configurations where heat exchangers are shared between the charging and discharging phase (i.e. hot storage, cold storage and recuperator) and employing a hot storage based on a sensible solid medium. The system design and performances are modelled in MATLAB, investigating the round-trip efficiency, the energy density and the system footprint across a wide range of operative conditions and adopting realistic assumptions for the plant components performance. The optimized results, obtained from hundreds of simulated cases, demonstrate that with moderately low cycle maximum pressures (around 150 bar) and low cycle maximum temperatures (below 130 °C), the battery can already achieve a round trip efficiency over 55 %, reaching maximum values greater than 60 % for low cold storage temperatures (−30 °C). Differently, the energy density largely benefits from increasing the maximum pressure up to 250 bar, thanks to larger temperature variation in the hot thermal storage. Under these conditions, the system footprint is lower than 20 m^2/MWh_{el}, with energy densities as high as 11 kWh_{el}/m^3 for a cold storage temperature of 0 °C.

1. Introduction

Long duration energy storage (LDES) systems are conventionally defined as electric storage technologies with a rated capacity higher than 8–10 h [1]. In recent years, the interest in the potential of these technologies has been rising considerably due to the soar in electrical production from non-dispatchable renewable energy sources, such as solar photovoltaic plants or wind farms. On the one hand, those sources have allowed to remarkably reduce the carbon intensity of the energy sector in high-income countries in the last 10 years (i.e. −38 % in the European Union, −37 % in the US, −18 % in China) [2], while, on the other hand, these are already facing challenges in exploiting their maximum potential due to bottlenecks in the electrical transmission system and mismatches between the renewable peak production and the load demand profile.

A significant amount of renewable energy curtailment is already affecting electrics grids with a strong penetration of renewables at local level. Clear examples include California, where the large increment in installed photovoltaic (PV) capacity led to a total renewable curtailment in 2023 of 2.66 TWh_{el} [3] (representing 6.6 % of the solar power availability), and China, where 14 % of word incremental PV capacity was installed in 2023. According to the latest data available for 2020, China experienced a total renewable curtailment equal to 45 TWh_{el}: while this value represents only 0.5 % of the total country electricity demand, it is the equivalent energy production of more than five 1 GW coal power plants operating at high capacity factor.

Even though the amount of energy curtailed in the last years was limited to 2–4 % of the energy transmitted in most countries [4], this fraction is expected to increase in the future [5], especially for those countries that are targeting decarbonization goals through new installations of PV and wind plants [6]. Investing in transmission grid improvements is generally one of the first actions, but these upgrades require substantial investments and long developments, making this solution effective only in few countries.

In this rapidly evolving scenario, also the energy storage market is undergoing a significant change, with several emerging technologies entering the market and positioning as solid competitors to consolidated solutions, namely pumped hydro energy storage (PHES) and battery energy storage systems (BESS).

In particular, PHES systems currently account for 94 % of the world electrical storage installed capacity [7] and, even if they are easily

* Corresponding author.
E-mail address: dario.alfani@polimi.it (D. Alfani).

https://doi.org/10.1016/j.enconman.2025.120269
Received 17 March 2025; Received in revised form 8 July 2025; Accepted 21 July 2025

Nomenclature

Acronyms

BEES	Battery Energy Storage Systems
CAES	Compressed Air Energy Storage
CCS	Carbon Capture and Storage
COP	Coefficient of Performance
ED	Energy Density
EER	Energy Efficiency Ratio
HTC	Heat Transfer Coefficient
HTF	Heat Transfer Fluid
HX	Heat Exchangers
LAES	Liquid Air Energy Storage
LCOS	Levelized Cost of Storage
LDES	Long Duration Energy Storage
LHES	Latent Heat Energy Storage
ORC	Organic Rankine Cycles
PCHE	Printed Circuit Heat Exchanger
PCM	Phase Change Materials
PHE	Primary Heat Exchanger
PHES	Pumped Hydro Energy Storage
PTES	Pumped Thermal Energy Storage
PV	Photovoltaic
RTE	Round Trip Efficiency
TCES	Thermo-Chemical Energy Storage
TES	Thermal Energy Storage

Symbols

A	Heat Exchanger transfer area [m^2]
h	Specific Enthalpy of the fluid [J/kg]
W	Mechanical energy [J]
Q	Thermal energy [J]
$\dot{Q}$	Thermal power [W]
p	Pressure [bar]
T	Temperature [°C]
Δp	Pressure drop across heat exchangers [bar]
Δt	Duration of the charge and discharge phase [h]
ΔQ	Thermal energy difference [J]
ΔT_{ml}	Mean logarithmic temperature difference [°C]
ΔT	Temperature difference [°C]
s	Specific entropy [kJ/kg K]
ρ	Density [kg/m^3]
c_p	Specific heat capacity [kJ/kg K]
$\dot{m}$	Mass flow [kg/s]
η	First law efficiency [-]
U	Overall heat transfer coefficient [W/m^2/K]
V	Volume of the system [m^3]
x_{bleed}	Fraction of the flow rate bled [-]

Subscripts and superscripts

cold	Cold storage
hot	Hot storage
rec	Recuperator
cycle	Power cycle
ch	Charging phase
dh	Discharging phase
eva	Evaporator
cond	Condenser

scalable to large scale sizes (from 100 MW$_{el}$ to 2 GW$_{el}$ of power [7]), present high round trip efficiencies (RTEs) in the range of 65 %-85 % [8] and the lowest levelized cost of storage (LCOS) among the various storage alternative technologies [7], they still present very high capital costs, long construction time and an intrinsic requirements related to soil orography and proper sites availability, limiting their potential in many countries. Differently, BESS do not suffer from geographical constraints and benefit from their inherent modularity, making them attractive for any size and for systems that requires a progressively expanding capacity. Nevertheless, BESS normally have discharge time in the order of few hours and suffer from ageing and wearing processes that, depending on the charging and discharging cycling pattern, may strongly limit their efficiency [9] and lifetime. Additionally, they require critical materials (cobalt, lithium and rare earths [10]) which are not easily available, with intrinsic ethical concerns related to working conditions in the extraction sites. However, BESS specific cost experienced a dramatic reduction between 2010 and 2020 dropping from around 450 $/kWh to around 100 $/kWh, and several projections indicate that their specific cost could fall below 75 $/kWh by 2027.

Considering the limitations of PHES and BESS, both researchers and industrial actors have worked to propose a large variety of LDES technologies that are now close to commercialization at utility scale. Gravitational energy storage as proposed by *Energy Vault* is one of the main technologies which has already been validated at 25 MW-100 MWh size. This solution is based on the use of electricity to lift blocks of concrete during the charging phase and lower them to ground level during discharging periods. The resulting RTE is potentially very high (up to 85 %), but issues related to the visual impact and the low energy density still represent a limitation of this technology. For this reason, different companies are focusing on underground installations in mines (e.g., *Mine Storage* and *SENS*) or high-density fluids (*RheEnergise*). Except for gravitational energy storage, all the other technologies under development are based on the use of either thermomechanical systems or pumped thermal energy storage (PTES).

The first class encompasses technologies where the storage of heat is combined with the storage of the working fluid in different thermodynamic states: examples of this category are compressed air energy storage (CAES), Liquefied Air Energy Storage (LAES) and CO_2 batteries™. CAES and LAES have a rated power that ranges from a few to hundreds of MW, with variable RTEs in the 40 %-70 % range, depending on the adopted technical solutions [11]. They are commercialized by companies such as *Hydrostor*, which is developing a 500 MW$_{el}$ CAES system with a storage size of 4 GWh$_{el}$ [12], and *Highview Power*, whose next project is a 200 MW$_{el}$ / 2.5 GWh$_{el}$ LAES system [13].

Another promising solution close to reach the commercial stage is the CO_2 Battery™ proposed by *Energy Dome*. Their system works by compressing and liquefying CO_2 during the charging phase and by evaporating and expanding it during the discharging phase. The process is achieved by storing the heat available from the working fluid at the outlet of the compressor in a thermal energy storage (TES) system during the charging phase, and later use it to evaporate and heat up the CO_2 flow in the discharging process, before the expansion in the turbine. According to the company, the rated capacity and RTE of the CO_2 Battery are 20 MW$_{el}$ and 75 %, respectively [14]. However, the main disadvantage of this technology is related to the need for a CO_2 storage system at ambient conditions that, given the low density of CO_2 at ambient temperature and pressure, entails large storage volumes, even if at low cost.

The second class, also called Carnot Batteries, defines systems where only heat is stored in a hot and/or a cold reservoir during the charging phase, and it is later exploited for reconversion into electrical power during the discharging phase. In these systems, the working fluid operates within a closed cycle.

PTES systems can potentially solve the drawbacks of the previously mentioned technologies for large-scale energy storage, such as CAES and PHES, since they do not require specific geological characteristics. Moreover, their operation is based on well-known thermodynamic cycles and established technologies, with the only significant issue related to the selection and design of the most appropriate TES systems [15]. Another possible advantage of PTES systems is related to the opportunity to store both heat and cold in the hot and cold TES, respectively, making them a suitable solution for sector coupling for users or energy communities that do not only require electricity, but also cooling [16] and heating [17], positively affecting the design of district heating networks [18]. In addition, during the charging phase, PTES systems can exploit an external waste heat source to boost their efficiency, or even absorb heat rejected appositely from another power cycle at low temperature [19]: literature works that proposed to recover heat from sensible and latent heat sources at 100 °C reported electrical RTE up to 100 % in thermally integrated configurations [20,21]. Various concepts for PTES systems have been conceived and proposed, using different working fluids and thermodynamic cycles. Thorough reviews of these potential solutions are available in the literature, such as the work of Dumont [15]. *Malta Inc.* has developed a technology based on a closed air Brayton cycle, with molten salts for the hot storage and a water-glycol mixture or *iso*-propane for the cold storage [22]. In 2022, *Southwest Research Institute* (SwRI) and *Malta Inc.* collaborated to assemble and commission the first pilot plant in San Antonio, Texas and the technology is now close the commercial stage. Studies on closed Brayton cycles were proposed by McTigue, among the others, assessing PTES competitiveness against BESS for storage durations above 6 to 8 h [23]. *Echogen Power Systems* and *MAN Energy Solutions* are focusing on CO_2 transcritical systems as those investigated in this work, while the use of Organic Rankine Cycles (ORC) is explored by different European projects [24–26] and proposed by *FutureBay*.

1.1. CO_2 Carnot battery state-of-the-art

Among the different PTES concepts, the development of transcritical CO_2 Carnot Battery systems is of particular interest for the potential synergies with other sectors that are gaining widespread attention from academia, industry and grid operators [27–30]. The adoption of CO_2 as working fluid for power production systems is currently studied in many applications that share with CO_2 Carnot Battery systems high pressures, turbomachinery operation close the critical point, such as in semi-closed internal combustion cycles for direct carbon capture and storage (CCS) implementation as, for example, the Allam cycle [31,32]. CO_2 Carnot Battery configurations are investigated in both supercritical (Brayton) and in transcritical (Rankine) layouts [33,34]. This work focuses on the latter, employing transcritical Rankine cycles for both the heat pump and the power cycle, which are coupled with a hot sensible and a cold latent Thermal Energy Storage (TES) system. The first example of this concept can be found in Mercangöz work, discussing a system with a multi-tank pressurized water hot TES and a latent cold TES based on ice [35]. Mercangöz also considered an external chiller to ensure the energy balance at the cold storage between the charging and discharging phases, whose importance is evidenced in this work. However, the work did not consider the possibility of using the same heat exchangers (HXs) for the charge and discharge phase of the battery. Under the hypothesis of no pressure drops and realistic turbomachinery isentropic efficiencies (turbine and compressor at 86 % and 81.5 %, pump and expander at 80 % and 80 %, respectively), the maximum RTE achievable has been estimated around 51 % for optimized configurations. Morandin have improved the analysis of those systems by implementing a design procedure based on pinch analysis for various cycle configurations, all sharing the same hot and cold TES [36,37]. This work also introduced the idea of ensuring the overall energy system balance by releasing heat to the ambient during any of the two phases, to avoid the need for an external chiller. The authors computed a maximum RTE of around 62 % with a recuperated cycle for both the charging and discharging phases, but considering no pressure drops, a complex hot TES adopting several Heat Transfer Fluid (HTF) loops and very low pinch point temperature differences, of around 4 °C. Ayachi was the first to study a different type of hot storage, as they considered a ground heat storage based on multiple isothermal columns, substituting the conventional multi-tank pressurized water system [38]. In their analysis the authors included pressure drops in the heat exchangers and presented a methodology to design the ground heat storage system: among the various solutions described, the one with the optimal RTE achieved a value of 55.8 %. A different solution was proposed by Kim, using isothermal compression and expansion, with a more theoretical perspective, reaching an optimized case with a RTE of 73 % [39].

CO_2 Carnot batteries are also being studied in the industry by companies such as *MAN Energy Solutions* [40,41], and *Echogen Power System* [42]. The first one is developing a system analogous to the one presented by Mercangöz [43] in collaboration with *ABB*, which also owns two patents for the technology [44,45]. Recently, they have also successfully commissioned a 70 MW_{th} heat pump system to decarbonize the heat supply of Esbjerg, in Denmark, with a district heating network. The system employs a compressor-expander transcritical CO_2 unit with the same architecture of their PTES system and it aims at providing 280 GWh_{th} to the district heating network each year [46]. Differently, *Echogen Power System* is investigating a high-pressure high-temperature system where solids, like sand or concrete, are used as the hot storage media. They recently partnered with *Westinghouse Electric Company* for the development of a 1.2 GWh_{el} LDES system based on a CO_2 PTES in Healy, Alaska. Once built and commissioned, it will be the largest single energy storage installation in the US [47,48].

1.2. Scope of work

This work aims to analyse in detail the abovementioned CO_2-based Carnot Battery system by focusing on a set of aspects that have not been investigated with a sufficient level of detail in the literature so far. Thus, this work presents a wide sensitivity analysis to strengthen the optimization process, with the following novel approaches:

- The inclusion of a hot storage based on a solid thermocline solution, marking a clear distinction with the multi-tank water storage generally considered in most of the current literature [35–37]. An analysis on the multi-tank storage ideal case is also included, and this is used as term of comparison.
- The use of a single component for each of plant heat exchanger (hot heat exchanger with hot TES, cold heat exchanger with cold TES and the internal recuperator), shared between the charging and discharging phase, allowing for a better understanding of the impact of heat exchangers off-design operation on the system performance. Due to the system high pressure, the recuperator is modelled as a printed circuit heat exchanger (PCHE), a technology well-known for its compact design and high thermal efficiency, which has been often associated with supercritical CO_2 power cycles [49].
- The CO_2-to-hot storage heat exchanger serves as heat rejection unit during the charging phase and as heat introduction unit during the discharging phase, and it is proposed as a solid matrix submerged with tubes where the CO_2 flows in supercritical state. Differently, the CO_2-to-cold storage heat exchanger works as an evaporator during the charging phase and as a condenser unit during the discharging phase, leading to a non-trivial reversible operation of this component from both technical and numerical perspective. This design choice significantly reduces the number of required components and the system overall capital cost. However, its numerical simulation requires a highly iterative approach and thus a computationally intensive model to solve the component off-design behavior.
- The study of two different solutions to ensure the cold storage energy balance after a complete charging-discharging cycle. The first solution adopts a chiller as previously proposed in the literature

[35,36,38], while the second one exploits a vapor bleeding as an alternative solution to reduce system complexity and avoid the electrical consumption of an external chiller.
- The investigation and identification of the optimal performance, including the maximization of the system energy density, through a comprehensive set of sensitivity analyses of the main components assumptions (such as the heat exchangers pressure drops and the isentropic efficiency of the turbomachinery), including an analysis on the cold storage temperature.

The ultimate objective of the work is to obtain performance and energy density maps of the investigated CO_2 Carnot Battery over a wide range of operating parameters set at design conditions, thus allowing to identify optimized trends for the system main design parameters (i.e. charging and discharging pressures). The results of this work can be used to define and support the design process of LDES systems based on transcritical CO_2 Carnot Battery and they also provide a fair comparison in terms of RTE and energy density against other competitive energy storage solutions.

2. CO_2 Carnot battery operating principle and adopted plant schemes

The T-s (temperature – specific entropy) diagrams of the charging and discharging phase of a CO_2 Carnot Battery are reported in Fig. 1. In both charging and discharging phase the system operates as a CO_2 transcritical cycle with a minimum pressure below the critical one, thus involving a phase transition process, and the maximum pressure higher than the critical one, thus involving a supercritical cooling or heating process.

During the charging phase, saturated vapor is heated up in a recuperator (1 → 2) before being compressed by the compressor (2 → 3). The high temperature supercritical CO_2 is cooled down releasing heat to the hot storage media (3 → 4) and, subsequently, further cooled down in the recuperator (4 → 5) where the low-pressure CO_2 is heated up (1 → 2). The cooled CO_2 is then expanded in a two-phase flow expander (5 → 6) down to the evaporator pressure, where energy is released by the cold storage to evaporate the working fluid (6 → 1).

During the discharging phase, the cycle progresses in the opposite direction. Saturated liquid is pressurized by a pump (1′→2′) and heated in the recuperator (2′→3′) before entering in the hot storage section, where the heat stored during the charging phase is used to increase the fluid temperature (3′→4′). The working fluid is then expanded in a turbine (4′→5′) before entering the recuperator (5′→6′) and then eventually in the condenser, where energy is released to the cold storage media by the condensation process (6′→1′).

The energy balance of the two thermodynamic cycles can be formulated for both the charging (in Eq. (1)) and the discharging process

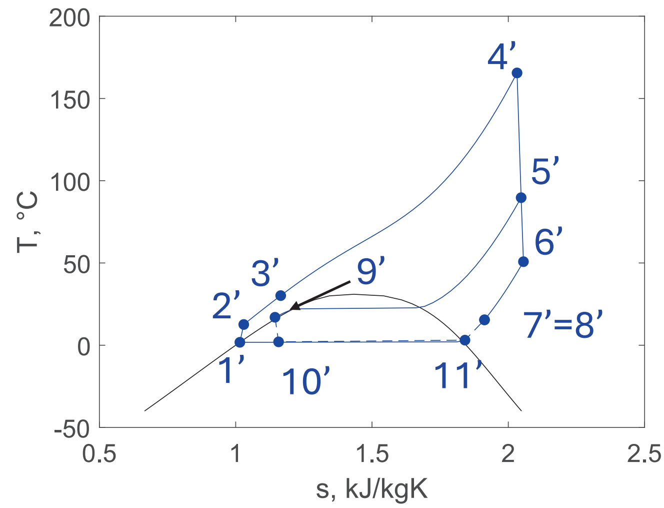

Fig. 2. T-s diagram of the discharging cycle of the Carnot battery with vapor bleeding architecture.

(in Eq. (2)) as follows:

$$W_{ch}^{net} + Q_{ch}^{cold} = Q_{ch}^{hot} \quad (1)$$

$$Q_{dh}^{hot} = W_{dh}^{net} + Q_{dh}^{cold} \quad (2)$$

where W_{ch}^{net} and W_{dh}^{net} are the net mechanical energy consumed and produced by the turbomachinery during the charging and discharging phases, respectively. The first one is computed as the difference between the energy consumption of the compressor and the energy production by the two-phase flow expander, while the second one is the difference between the energy produced by the turbine and the energy consumption of the pump. Moreover, Q_{ch}^{hot} and Q_{dh}^{hot} are the energy exchanged with the hot storage during the charging and the discharging phase, respectively, while Q_{dh}^{cold} and Q_{ch}^{cold} refer to the heat exchanged with the cold storage during the condensation and the evaporation process. If the energy stored in the hot storage during the charging phase is completely exploited in the discharging phase, the two equations can be combined to obtain Eq. (3):

$$W_{ch}^{net} - W_{dh}^{net} = Q_{dh}^{cold} - Q_{ch}^{cold} = \Delta Q_{balance}^{cold} \quad (3)$$

While the Carnot battery round trip efficiency (RTE), can be computed as Eq. (4):

$$RTE = \frac{W_{dh}^{net}}{W_{ch}^{net}} \quad (4)$$

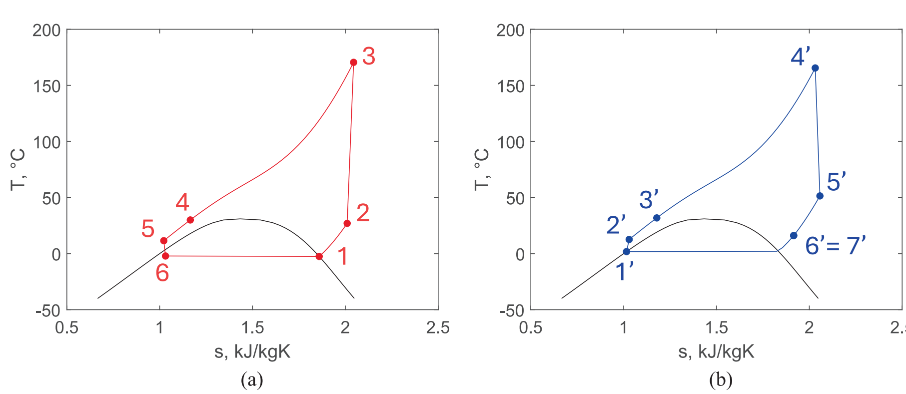

Fig. 1. Temperature-specific entropy (T-s) diagrams of the charging (a) and discharging (b) cycle of the CO_2 Carnot battery. In the reported discharging cycle the heat rejection unit is not implemented. Consequently point 6′ overlaps with point 7′.

Evidently, if the mechanical energy produced during the discharging phase is lower than the energy consumed during the charging one over a full cycle (i.e., RTE < 100 %), the heat released to the cold storage during condensation exceeds the one absorbed during evaporation, leading to an energy imbalance at the cold storage. To solve this problem and to ensure system cyclability, two different system architectures are considered in this work as reported in Fig. 3 and Fig. 4.

- Chiller –based scheme (Fig. 3): It consists in the inclusion of a conventional vapor compression chiller to ensure the energy balance of the cold storage by rejecting the excess heat released in condensation during the discharging phase. It must be noted that this additional consumption affects the RTE on a different extent depending if it occurs during the charging or discharging phase, but also results in different impact on the system economics. From an operative cost perspective, it is reasonable to operate the chiller during charging periods, where off-peak electricity is abundant at low price (or even negative price), rather than reducing the power output during discharge, when the reduction of power injected to the grid can strongly penalize the revenues. On the contrary, considering the impact on the investment cost the use of the chiller during discharge periods allows to reduce the size of the cold storage that can be designed on the charging operation rather than on the discharging one, with a potentially high impact on cost reduction and energy density increase (up to + 10–15 %). In this work, techno-economic performances are not quantified and the tradeoff among the two effects shall be investigated by the adoption of the LCOS as a figure of merit. Thus, the optimal case could adopt one or the other approach depending on the specific cost of the components, the electricity price in charging mode and the number of cycles per year. The RTE is here calculated considering the consumption during discharging phase, as it leads to a more conservative value. On the other hand, this approach enables a higher energy density by reducing cold storage volume and ensures a more consistent comparison with the vapor bleeding case, where the penalization is intrinsically considered in the discharging phase. Depending on the selected operating conditions, considering the chiller consumption during the charging process would result in a net RTE increase

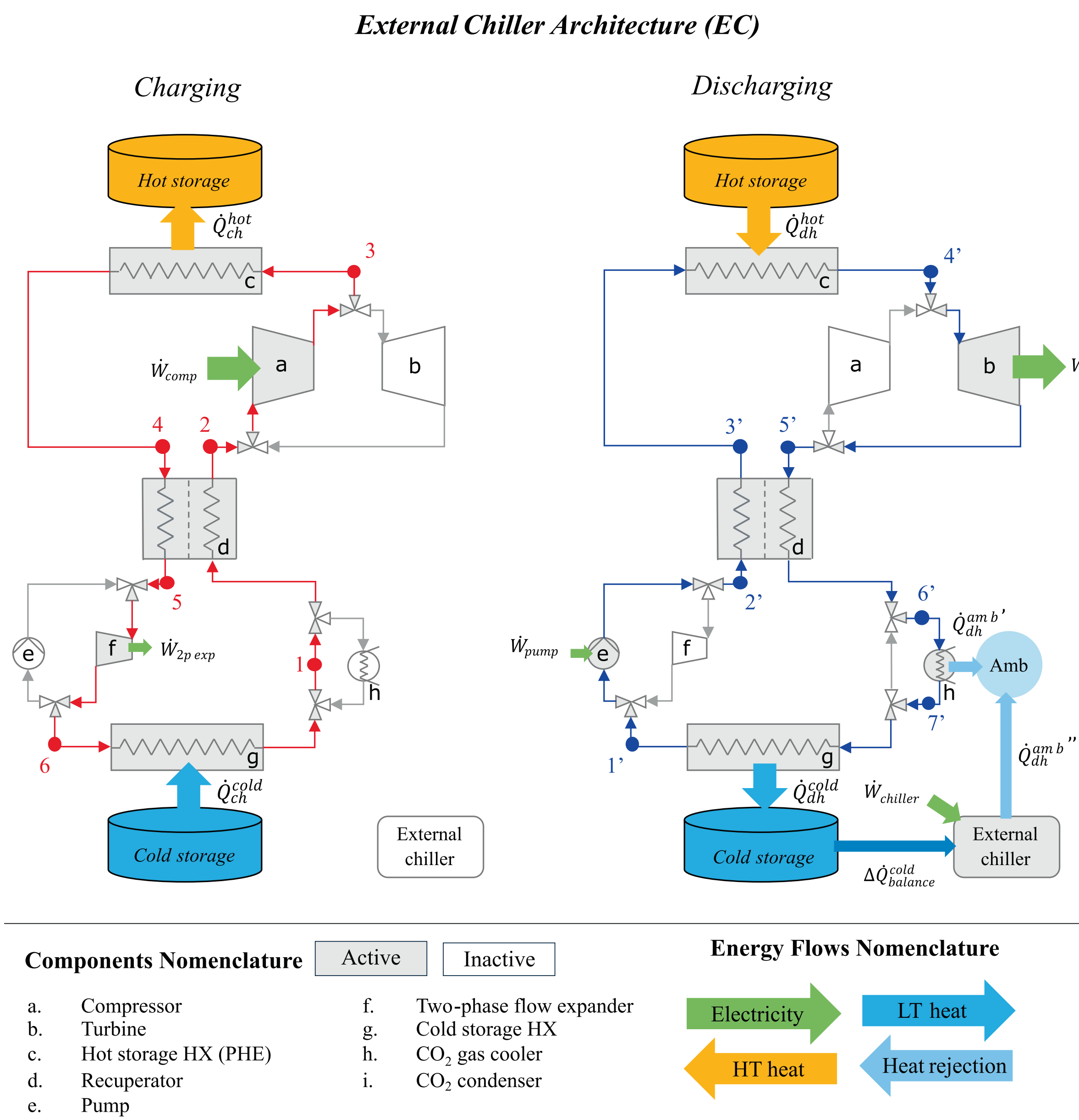

Fig. 3. Plant configuration of the CO_2 Carnot Battery adopting an external chiller.

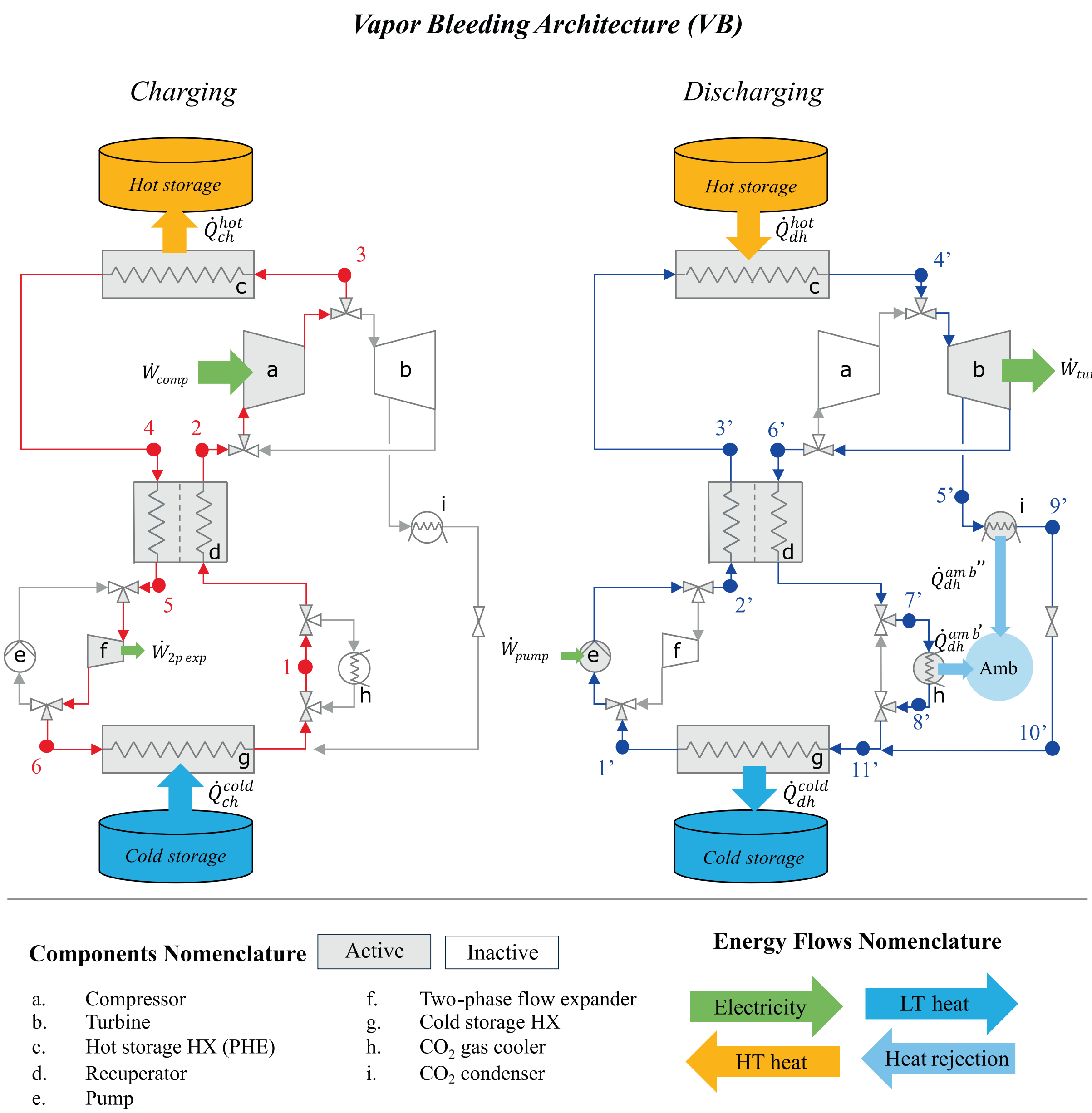

Fig. 4. Plant configuration of the CO_2 Carnot Battery adopting vapor bleeding.

between 2 and 5 percentage points compared to the case where this component is employed in the discharging phase.

- Vapor bleeding-based scheme (Fig. 4): It employs a vapor bleeding from the turbine, which is subsequently condensed at a temperature higher than the ambient one, rejecting heat directly to the environment and thus leading to a reduction of the heat released to the cold storage. Releasing heat to the environment changes the system overall energy balance from Eq. (3) to Eq. (5), where it is evident that the amount of heat released can be tuned to be equal to $W_{ch}^{net} - W_{dh}^{net}$ and thus to ensure the cyclic energy balance of the cold storage ($\Delta Q_{balance}^{cold} = 0$). This thermal energy can be theoretically rejected into the environment during any of the two phases; however, operating by condensing part of the CO_2 mass flow with the ambient allows for the minimum average temperature of heat release, thereby minimizing the RTE penalization.

$$W_{ch}^{net} - W_{dh}^{net} - Q_{amb} = Q_{dh}^{cold} - Q_{ch}^{cold} = \Delta Q_{balance}^{cold} \tag{5}$$

The T-s diagram for the second architecture discharge phase is reported in Fig. 2, with the additional condensation process ($5' \rightarrow 9'$). This stream is then expanded to the minimum pressure ($9' \rightarrow 10'$) and mixed with the remaining part of the CO_2 exiting the recuperator before entering the low temperature condenser ($7'$, $10' \rightarrow 11'$). A throttling valve is adopted in this case rather than a two-phase flow turbine according to the low pressure ratio involved.

Both solutions depicted in Fig. 3 and Fig. 4 introduce a RTE penalization with respect to plant configurations that don't enforce the energy balance at the cold storage: in the first case due to the chiller electrical consumption, in the second case due to the reduction of mass flow rate in expansion and the additional auxiliary consumption of the condenser fan or circulation pump: nevertheless, both approaches ensure a more accurate calculation of system performance.

An additional strategy investigated in this work to increase the RTE consists in implementing an additional heat rejection unit, operated when the recuperator outlet temperature is higher than the ambient one, to reduce the temperature of CO_2 before entering the condenser, thus reducing the consumption of the chiller in the first configuration and the bled vapor fraction in the second one. In this case, temperature of point $7'$ is lower than $6'$ in Fig. 1 (right), and temperature of point $8'$ is lower than 7′ in Fig. 2.

The next subsections focus on the technological description of the main subsystems, namely: the hot storage, the cold storage and the turbomachinery.

2.1. Hot storage system

Due to the real gas effects that arise in supercritical isobars, the CO_2 temperature profile across the heat exchanger with the hot storage is highly nonlinear, especially for pressures close to the critical one in the lower temperature range. A common solution for the thermal storage that aims at providing a good matching between charging and discharging temperature profiles is the use of a multi-tank system (as also implemented by *MAN Energy Solutions* [50]), where multiple tanks at different temperature levels are employed. A schematization of this storage system is reported in Fig. 5 for the charging phase, while during the discharging phase all stream directions are just reversed.

This solution allows to adapt the HTF mass flow rate (and thus slope on the temperature-thermal power diagram) to the CO_2 stream heat capacity, that depends on the local value of constant pressure specific heat capacity. Fig. 6 helps to visualize the impact of the number of storage tanks on the temperature profiles of the primary heat exchanger (PHE) and the resulting RTE: both cases are optimized in performance and adopt the same maximum pressure of 150 bar for both the charging and discharging phases. Fig. 6**.a** adopts a two-tanks system and thus a single HTF mass flow in a single heat exchanger, while Fig. 6**.b** adopts four tanks and three heat exchangers in series. It is possible to appreciate that fixing inlet temperatures for both the fluid in charge (outlet of the compressor) and fluid in discharge (outlet of the recuperator), the case with 4 tanks allows to increase the turbine inlet temperature by 3 °C and the RTE by 3.5 percentage points.

This proposed multi-tanks solution has been extensively investigated in the literature [35–37]: it assumes that the temperature of each tank remains constant during both the charging and discharging processes, thus fixing the temperature profiles in both phases, and consequently the mass flows, ensuring a correct cyclic operation. This approach may result in a non-trivial system control procedures when the plant runs at part load or when the system does not complete the cycle before starting the next charging phase. In particular, issues may arise more drastically with lower maximum pressures of the two thermodynamic cycles, as the variation in specific heat is more pronounced. On the other hand, if the system is designed for high pressures (i.e., 250 bar), with a minimum temperature of the storage above 70 °C-100 °C, then the impact of real gas effects is rather limited, and a good temperature match can be obtained already with a dual HTF loop system. This latest concept has been proposed by *Echogen Power Systems,* with a first HTF level (up to 150 °C) using pressurized water which is then stored in a liquid thermocline vessel, and the second HTF level running with thermal oil (required because the high maximum temperature at compressor outlet equal to around 300–350 °C) which then releases heat to a packed bed to reduce the amount of costly and flammable oil.

Moreover, the multi-tanks thermal storage solution leads to adequate overall RTE only when the charging and discharging CO_2 temperature

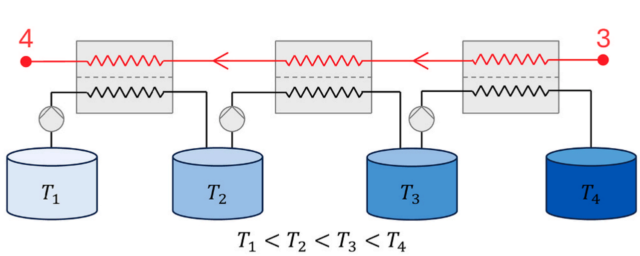

Fig. 5. Schematization of a multi-tank storage system during the charging phase. During the discharging phase all streams direction are reversed.

profile are similar, and thus it is suggested for configurations with similar charging and discharging cycles maximum pressure. Fig. 7 depicts three representative PHE temperature profiles imposing the same inlet and outlet temperature during charge (red line) and the same inlet temperature during discharge (blue line) and adopting, to generalize the conclusion, an ideal multi tanks storage system composed of an infinite number of tanks. All the three conditions in Fig. 7 are simulated with a pinch point temperature difference of 5 °C between the two temperature profiles.

In the case of $p_{dh} > p_{ch}$ (Fig. 7**.**left), large temperature differences between the two profiles are unavoidable due to the different CO_2 heat capacities at different pressures near the critical point. Consequently, a large terminal temperature difference is obtained at the hot end, leading to a lower turbine inlet temperature which in turn involves a strong a penalization of the discharging cycle efficiency. Differently, the case of $p_{ch} > p_{dh}$ (Fig. 7**.**right) does not preclude high turbine inlet temperatures, but the lower expansion ratio leads to a reduction of the turbine work, and so of the RTE.

It must be noted that decoupling the temperature profiles of the two phases would allow to increase the turbine inlet temperature in the case depicted in, thus increasing the RTE of configuration characterized by $p_{dh} > p_{ch}$.

Technically, this can be done by replacing the hot storage with a solid sensible material, such as rocks or sand-like solids. During the charging phase the solid matrix is heated up by the hot CO_2 exiting the compressor: stored heat is then released by heating the CO_2 exiting the recuperator (or the pump, if this component is not present), basically working as a solid-phase thermocline. This solution thus unlocks the possibility to completely decouple the temperature profiles of CO_2, and to adopt discharging pressures higher than the charging one while keeping similar terminal temperatures in the two operation modes [51]. This effect is reported in Fig. 8, depicting the fluid temperature profile during charge and discharge. It must be noted that the crossing between the two profiles is possible since the heat exchange process occurs in two different moments. On the other hand, to avoid that the temperature gradient reaches one of the two ends of the storage, thus implying a temperature decrease at turbine inlet and a penalization in performances, a proper overdesign of the solid material is required: this would however have little impacts on the overall system costs, since the material used as solid medium are generally selected to be inexpensive.

The most common architectures used for this storage technology are the packed bed and the solid matrix [52]: packed beds are tanks filled with packing materials consisting of rocks, ceramics or minerals, that during the charging and discharging phases allow for heat transfer between the storage and the working fluid by letting the fluid flow in the voids between the filling elements. The second option is characterized by storing heat in a module composed of a solid matrix usually made of concrete, steel, or graphite [52], with embedded fluid channels or tubes where the fluid flows transferring heat to the surrounding material. In principle, both solutions are suitable in Carnot battery systems where the working fluid in the charging phase is the same as the one in the discharging phase, as in this work.

The first option allows for a much higher specific heat transfer area per unit of volume compared to the second case, with a heat transfer process that is mostly affected by convection, leading to steeper thermoclines, and thus to a more compact storage system [53]. However, packed beds shall be excluded for this specific application due to their inability to withstand the high pressures required by CO_2-based PTES, which easily exceed 100 bar. Differently, a solid sensible matrix employed as hot storage adopts small diameter metal tubes, limiting the risk of failure, while unfortunately leading to less effective heat transfer processes because of the limitation due to conduction in the solid material. Additional issues could be related to the solid matrix thermal fatigue due to cycling process of thermal expansion and contraction that may cause cracks and voids that would further limit the global heat transfer coefficient [54]. This second solution, with a concrete matrix as

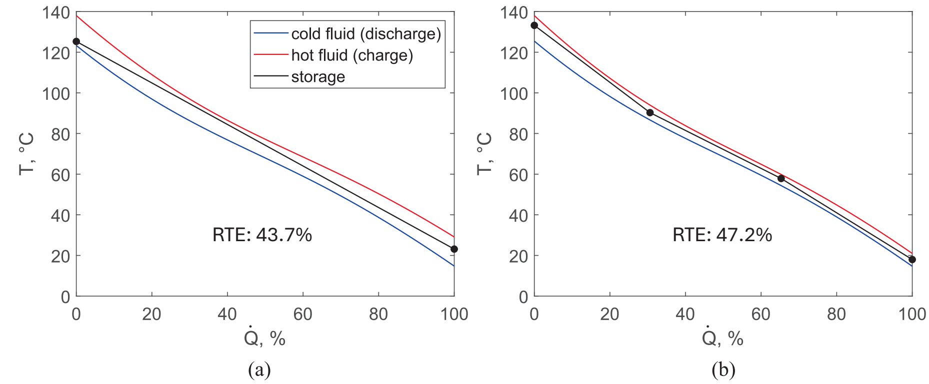

Fig. 6. T-Q diagrams of the hot storage HX for Carnot battery configurations with a 2-tanks (a) and 4-tanks (b) TES system (p_{ch}: 150 bar, p_{dh}: 150 bar).

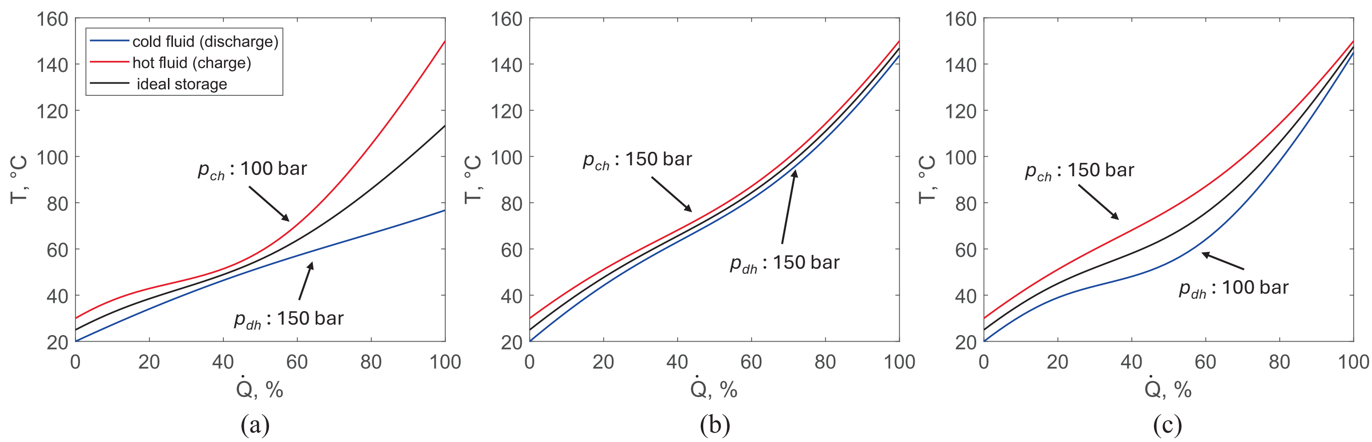

Fig. 7. T-Q diagrams of an ideal hot storage HX based on a liquid medium for CO_2 Carnot battery configurations at different maximum pressures of the charging and discharging phase. Condition with $p_{ch} < p_{dh}$ (a), $p_{ch} = p_{dh}$ (b), $p_{ch} > p_{dh}$ (c).

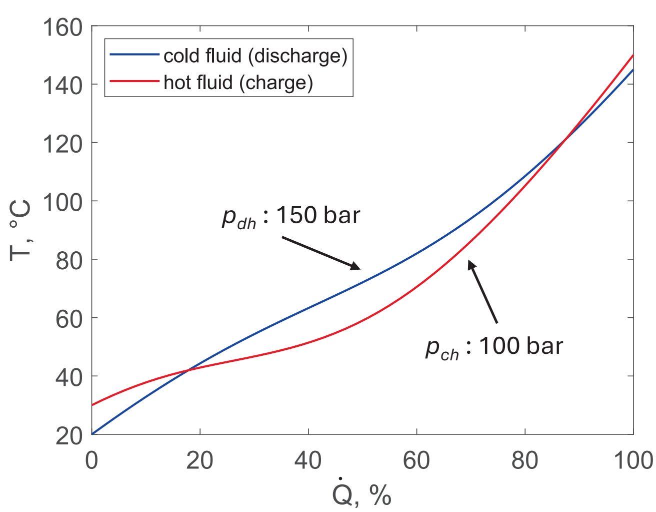

Fig. 8. T-Q diagram of a hot storage HX for configurations of Carnot batteries with solid medium hot storage.

hot storage, was firstly adopted by *Echogen Power System* for their project in collaboration with *Westinghouse Electric Company* [47] and it is the one considered in this work. In particular, concrete is considered as the storage medium.

2.2. Cold storage system

In order to properly store heat in the cold storage, a constant-temperature thermal storage is considered the best option for the coupling with the isothermal evaporation and condensation processes of carbon dioxide: regarding this, two technologies available for storing energy at a constant temperature are thermo-chemical energy storage (TCES) and latent heat energy storage (LHES) [7].

In TCES, heat is introduced and rejected through the dissociation and re-association of molecular bonds in a fully reversible chemical reaction [55]. In contrast, LHES stores and releases energy through the melting and freezing of a medium known as phase change material (PCM). While TCES offers higher energy density than LHES [55], the technology is more complex and not completely commercially employed [55]. On the other hand, LHES is a more established technology [31] and it is the option used in previous studies on CO_2 PTES systems [35–38] and thus adopted in this work.

Different technological options for LHES have been presented in the literature and mainly classified depending on the PCM confinement. The most common solution is to have the PCM in the shell-side of a shell & tubes heat exchanger [56,57], lowering the cost but also leading to a reduction of heat transfer performances due to the increasing thickness of the solid layer [57]. Complex finned geometries are proposed in the literature [57], limiting this problem and reducing the volume of PCM pockets, while at the same time involving additional issues due to mechanical stresses on metal surfaces related to material volume variation during phase change. Another commercially available option involves storing energy using capsules filled with PCM suspended in a thermal bath [58]. This option allows to significantly increase the heat transfer rate by reducing the thermal resistance associated with the formation of the solid layer [33]. In particular, macro-encapsulation offers the ability to enhance component performance while maintaining cost-effectiveness, as proposed by companies like *Thermofin*, which is currently offering heat transfer equipment based on this concept [59]. A final option, as proposed by *Echogen Power Systems* is to use a slurry of ice and water which circulates on the heat exchanger tube bundle. In this case it is not possible to exploit the whole latent heat of phase transition since too high solid fraction would involve difficulties for slurry circulation, leading to an excessive increase of the storage volume.

Consequently, a LHES based on encapsulated PCM has been adopted in this study. Specifically, a shell & finned tubes architecture with the capsules suspended in a thermal bath in the shell side is considered. Different PCM must be employed for the different cold storage temperatures that are investigated in the sensitivity analysis: for temperatures down to −21.2 °C mixtures of water and NaCl can be used, while for temperatures down to −30 °C a wide range of commercial solutions are available [58]. Thermal bath circulation auxiliaries are not considered in this work.

2.3. Turbomachinery modelling

The performances of the four turbomachinery are characterized in this work with a simplified zero-dimensional approach, through the definition of their isentropic efficiency. Isentropic efficiencies allow for the calculation of the outlet conditions of the turbomachinery given the inlet ones and the adopted equation of state, which for carbon dioxide is the Span and Wagner equation of state [65]. As only steady-state and nominal operation are considered for both cycles, no maps or curves for the off-design performance of the turbomachinery are necessary.

In this work, a reference charging power of 50 MW_{el} has been considered for the system design. For the charging cycle, the main turbomachinery is the compressor, and an axial architecture is selected according to the required mass flow rates and efficiency considerations. Axial compressors are well-suited for large-scale power applications as they can handle higher flow rates with relatively high isentropic efficiencies, typically in the range of 85–90 %, and in this work a reference isentropic efficiency of 85 % is thus considered [60]. It must be noted that, thanks to the adoption of the recuperator, the compressor always operates with superheated vapor at the component inlet, thus without possible risks of liquid droplets formation.

Similar considerations can be drawn for the discharging phase, where an axial turbine is selected with a reference isentropic efficiency equal to 90 % [60]. For sake of simplicity, efficiency penalties for the turbine caused by the formation of liquid droplets are not considered in cases where the expansion enters the saturation curve.

Additionally, during the charging phase, a two-phase expander is used to recover energy, based on the solution employed in the *MAN Energy Solutions* ETES system, a proven PTES system that utilizes CO_2 as the working fluid. Compared to a more conventional throttle valve, the use of an expander significantly mitigates exergy losses and enhances system efficiency, as studied in detail in section 5.4.1. A two-phase expander isentropic efficiency equal to 80 % has been considered in this work. As experimental data validating this component efficiency is currently not available in literature, the isentropic efficiency has been chosen based on similar works on CO_2 PTES systems [35,36,61].

Finally, in section 5.4.2, the study proposes a sensitivity analysis on the state-of-the-art of the turbomachinery manufacturing technology by introducing a variation on the value of their isentropic efficiency.

3. System numerical modelling

The investigated systems are designed to characterize various configurations of a Carnot battery with a net electric power of 50 MW_{el} during the charging phase, as representative of a commercial scale plant. The charging and discharging times adopted are equal to 10 h, a value coherent with most analogous systems developed by the industry in the LDES field, such as *Energy Dome* and *Echogen Power systems* [1,5].

An ad-hoc numerical tool has been developed in MATLAB for the design, the simulation and the optimization of the CO_2 Carnot battery technology, described in the following subsections. The thermodynamic and transport properties of the working fluid are computed with calls of REFPROP V.10 directly in MATLAB, adopting the Span and Wagner equation of state [62].

The overall methodology adopted in this work is summarized in the flowchart proposed in Fig. 9. The approach consists of first simulating the charging phase and sizing the heat exchangers accordingly, as discussed in detail in section 3.1. The discharging phase is then solved iteratively by finding the CO_2 mass flow rate and thermodynamic conditions that result in the same HX geometry, as explained in section 3.2.

Out of the possible free design variables, three of them have been identified for the system optimization process and are handled by an optimization algorithm: the charging maximum pressure (p_{ch}), the discharging maximum pressure (p_{dh}), and the temperature at the PHE outlet during the charging phase (T_4). Each design variable lower and upper bound is reported in Table 1.

Regarding p_{ch} and p_{dh}, the lower bound has been chosen to operate the cycle relatively far away from the critical pressure (73.8 bar), to avoid the risk of phase change inside the hot storage system during a possible part load or transient operation, while the upper bound has been chosen to avoid excessive maximum pressures and it is taken accordingly to the maximum operative pressure of sCO_2 power plants [63]. For T_4, the upper bound has been chosen to be significantly higher than the optimal value for all the analysed cases and always checking that the optimal solution does not coincide with the selected upper bound.

For each case, both the configuration with the chiller and with vapor bleeding are analysed and optimized. The optimization procedure is carried out in two different ways: at first, by parametrically varying p_{ch} and p_{dh} and finding the optimal value of T_4, which produces results in the form of heatmaps; secondly, by determining the optimal p_{dh} and T_4 for each value of p_{ch}, which provides results focused on the optimal region. For the optimization procedure the *patternsearch* algorithm from the MATLAB optimization toolbox [64] has been selected, as its heuristic nature suits the discontinuous and non-differentiable nature of the problem, allowing for the best compromise between computational time and accuracy of the solution.

The following key performance indexes have been selected for the optimization of the system:

i. The RTE, defined as the ratio between the electrical energy produced along a full cycle during the discharging phase and the respective electrical energy required by the system in charging phase, as defined in Eq. (4).
ii. The system energy density (ED), reported in Eq. (6), calculated as the ratio between the overall electric energy released in a complete discharging cycle (lasting for a timespan Δt_{dh}) and the total volume of the system.

This latter parameter has been quantified calculating the mass of concrete and PCM required by the hot and cold storage, assuming an overdesign factor of 1.3 for the hot storage to account for thermocline breakthrough [53] and an encapsulated PCM void fraction equal to 0.5 for the cold storage according a packed bed structure [58]. Additionally, to compute the energy density, the recuperator volume computed in the sizing routine is added to the volume of the system, while for sake of simplicity it was assumed that the turbomachinery and the auxiliary chiller can fill in three containers (6 m x 3 m x 3 m).

$$ED = \frac{\dot{W}_{net}^{dh} \cdot \Delta t_{dh}}{V_{hot} + V_{cold} + V_{rec} + 3\,V_{container}} \tag{6}$$

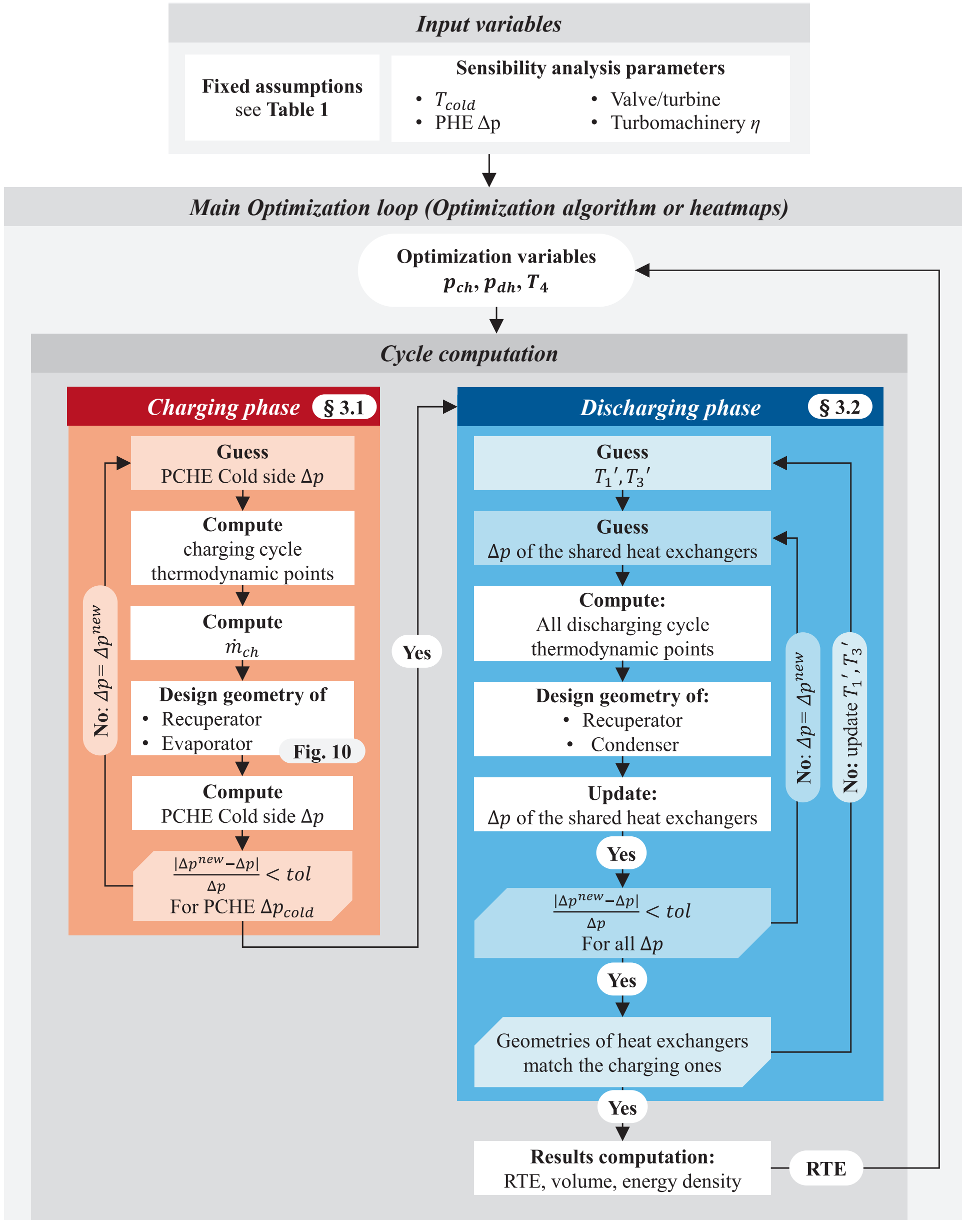

Fig. 9. Flowchart of the simulation and optimization procedure for the CO_2-based Carnot Battery system with heat exchangers shared between charging and discharging phase. Input variables consist in fixed assumptions and quantities varied in the sensitivity analysis; optimization variables can be handled performing a parametric analysis within a fixed range or by an optimization algorithm.

Table 1
Design variables upper and lower bounds.

Design variable	Lower bound	Upper bound
p_{ch} [bar]	80	250
p_{dh} [bar]	80	250
T_4 [°C]	T_{cold}	T_{cold} + 100 °C

All the assumptions related to the design and simulation of the base case are reported in Table 2, categorized according to the phase in which they are applied.

On average, PCM present densities of 1000–1200 kg/m^3 and latent heat in the range 250–300 kJ/kg, leading to competitive energy densities of around 70–90 kWh/m^3, compared to the 84 kWh/m^3 of water ice. For simplicity, in this work, a constant energy density of 85 kWh/m^3 was chosen as an average value for the range from 0 °C to −30 °C [58].

For all the simulations carried out in this work, any thermal loss from the thermal storages to the environment is neglected. This simplifying assumption is employed as thermal losses are dependent on the time duration of the standby process between the charging and discharging phase, which is expected to be lower than a day, and the insulation layers of the storages that are assumed to be sufficiently effective.

As mentioned in the previous section, in the base case configuration the energy balance at the cold storage is ensured by adopting an external chiller (Fig. 4, left). Its electrical consumption is calculated from the ideal reversible energy efficiency ratio (EER) and assuming a second law efficiency equal to 45 % [65–67] in order to adapt the chiller performance to the temperature span in case of low temperatures of the cold storage.

Finally, a series of sensitivity analyses are carried out, providing a more generalized understanding of the performance of these systems by varying the values of some of the input data from Table 2:

Table 2
Simulation assumptions at design conditions.

Parameter	Value	Defined in:
Recuperator pinch point ΔT, °C	5	Charging phase
Recuperator pressure drop	2 %	
Evaporator/condenser pinch point ΔT, °C	2.5	
Evaporator/condenser pressure drop	1 %	
PHE pressure drop	1 %	
Compressor isentropic efficiency	85 %	
Expander isentropic efficiency	80 %	
Concrete density, kg/m^3	2400	
Concrete thermal capacity, kJ/kgK	0.98	
PCM energy density, kWh/m^3	85	
Motor electro-mechanical efficiency	97 %	
PHE terminal ΔT, °C	5	Discharging phase
Turbine isentropic efficiency	90 %	
Pump isentropic efficiency	75 %	
Ambient temperature, °C	15	
Ambient condenser temperature, °C	20	
Cooler outlet temperature, °C	20	
Chiller 2nd law efficiency	45 %	
Generator electro-mechanical efficiency	97 %	

- Two cold storage temperatures (T_{cold}) equal to −30 °C and 0 °C (baseline value) are considered according to the minimum temperature of commercially available PCM and the use of water–ice mixture, as proposed by both *MAN Energy Solutions* and *Echogen Power Systems*.
- The turbomachinery efficiency, considering a net ± 5 percentage points on the baseline value
- The pressure drops in the PHE, considering an increase from 1 % to 5 % of the pressure at its inlet
- The adoption of a more conventional throttling valve with respect to the two-phase flow expander in the charging cycle.

3.1. Charging cycle definition and sizing of the HX

As the necessary input variables for the definition of the charging cycle (the heat pump) are defined, either through a parametric analysis or by an optimization algorithm, the MATLAB model computes the thermodynamic conditions of the working fluid in the charging phase by defining the temperatures, pressures and thermodynamic properties of each point according to the assumptions reported in Table 2. The area of each heat exchanger is calculated with a discretized 1-D method that computes the heat transfer coefficient (HTC), and the number and length of the channels (or tubes) needed to properly satisfy the assumptions on the pressure drop and thermal performances. Table 3 reports the adopted heat transfer and pressure drops correlations for the CO_2, both for single phase and two-phase conditions. Different correlations could have been adopted, but their influence on the final results would be limited to the actual size of the heat exchangers, and not on the system performance (in particular for the discharge operation) and its optimization.

More specifically, each heat exchanger has been discretized into 50 sections with equal heat duty, requiring a numerical routine that iterates from the guess of the CO_2 mass flux (kg/m^{2}s) and the assumption of channel hydraulic diameter, with the exception of the PHE with the hot storage which off-design is discussed in section 3.2. Given the temperature and pressure profile in the heat exchanger, the fluid velocity is calculated in each section, and the local friction factor and convective HTC are determined adopting the correlations reported in Table 3. Once the overall heat transfer coefficient (U) of each section is computed, the length of each section of channel or tube is calculated to match the target heat duty. Once the length of the channel is known, the total pressure drop is directly computed. Consequently, an iterative procedure is needed to find the number of channels that satisfy the pressure loss requirements. This procedure is schematized in Fig. 10 and represents the *'design geometry'* block of Fig. 9.

Regarding the cold storage heat exchanger, a shell & finned tubes architecture has been defined, with CO_2 flowing on the tubes and encapsulated PCM suspended in a thermal bath filling the shell side. Consequently, additional hypothesis must be considered to compute the heat transfer coefficient on the shell side. Since melting and solidification processes are unsteady by nature, defining a value for heat transfer coefficient between the PCM bath and the tubes external surfaces is not a trivial task, and it would require computationally expensive time-dependent models. To avoid this additional complexity, a constant value of 100 W/m^{2}K was assumed for both the charging and discharging phase according to the most similar case-study found in the literature [73,74].

It must be however noted that, for the scope of this work, the actual value of the external heat transfer coefficient has a negligible impact on the results, as this study aims to simulate and evaluate a system using the same heat exchangers during both phases. A variation in the value of the external convective heat transfer coefficient on the shell-side would surely lead to different heat exchanger surface, but the effect on the performance of the component during the discharging simulation would be negligible, as the component design carried out during the charging phase would change consistently. The geometrical parameters used for the design and simulation of the component are taken from the literature [63].

On the other hand, for the recuperator modelling, a PCHE architecture with straight channels was adopted. The same number of channels and the same diameter was assumed for the hot and the cold side. The number of channels were chosen to ensure that the cold side pressure drop during the charging phase match the value reported in Table 2. Consequently, the hot side pressure drop cannot be fixed during the charging phase but must be computed iteratively as a consequence. The geometrical parameters used to size and simulate the component taken from the literature [63]. While the recuperator is always present in the charging phase, this component is bypassed during the discharge phase if its operation is unfeasible, namely for those cases where the CO_2 turbine outlet temperature is lower than the CO_2 temperature at pump outlet.

3.2. Discharging cycle definition and off-design of the components

During the discharging phase simulation, the values of T_1', T_3' and the heat exchangers pressure drops are initially guessed and used to compute the conditions of the power cycle, as shown in Fig. 9. Afterwards, the heat exchangers are designed according to this new thermodynamic cycle through the procedure shown in Fig. 10 (excepting for

Table 3
Heat transfer and pressure drop correlations adopted for the modelling of carbon dioxide.

Heat Exchanger	Fluid conditions	Convective heat transfer	Frictional pressure drop
Recuperator	CO_2 high pressure liquid CO_2 low pressure vapor	Gnielinski [68]	Chen [69]
Hot storage HX	CO_2 high pressure supercritical	Gnielinski [68]	Chen [69]
Cold storage HX	CO_2 evaporation (charging)	Liu and Winterton [70]	Friedel [71]
	CO_2 condensation (discharging)	Cavallini [72]	Friedel [71]

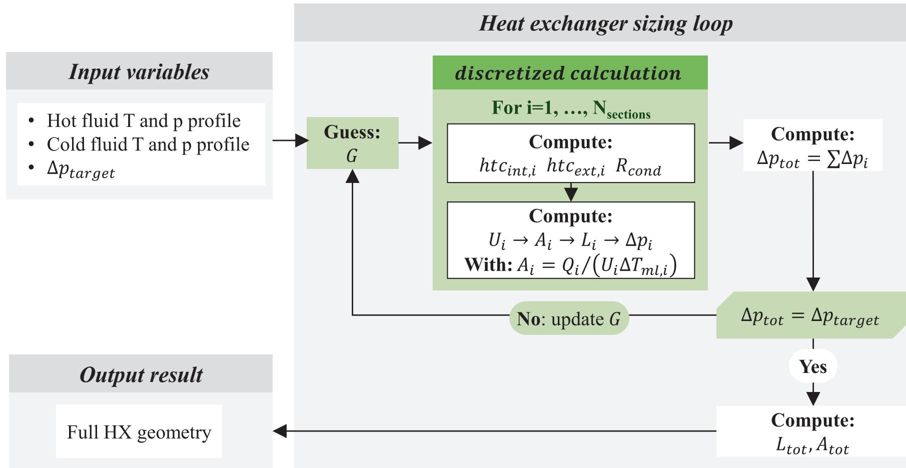

Fig. 10. Methodology for the design of the heat exchangers.

the CO_2 mass flux which is computed based on the number of tubes obtained in the design phase for each HX) and new pressure drops are evaluated. At this point, the pressure drops initially guessed are updated with these new values and this loop is repeated until convergence. A subsequent check on the heat exchangers areas is then performed, eventually updating the values of T_1', T_3' iteratively to satisfy these constraints. This computationally expensive approach, even if already employed for ORC-based solutions [75], represents a novelty in the literature for CO_2 Carnot batteries and it allows to compute the performance of the system in the power cycle considering the design carried out in the previous phase: under this perspective, neither the pinch point temperature differences nor the pressure drops values are assumed in the heat exchangers during the discharging phase, thus resulting in a more realistic assessment of the system performance.

While performing the power cycle simulation as discussed, additional simplifying assumptions were made regarding the hot storage PHE to avoid the need of solving unsteady-state models, necessary for the proper computation of the thermal profile across the solid matrix during the charging and discharging process.

During the discharging phase, most of the storage mass is initially at the temperature of compressor outlet (point 3), thus fluid exiting the storage (point 4′) is reasonably very close to this temperature for a consistent fraction of the discharging period, due to the very high heat transfer rate. Only when the thermal front of the thermocline gets at the hot end of the storage, finally the turbine inlet temperature starts decreasing, even if the temporal extent of this temperature decay is dependent on the storage overdesign. Analogous considerations are valid also during charging operation, related to the storage cold end and points 4 and 3′.

Considering the system design procedure of this work, a fixed average terminal temperature difference is assumed, as reported in Table 2. This condition is always feasible with a sufficient component oversizing, avoiding penalizing excessively the economic effectiveness of the plant, being the solid medium cheap and largely available. The working fluid frictional pressure losses on the other hand, are evaluated by fixing them during the charging phase and recomputed for the discharging one with Eq. (7) [63], derived from the direct application of the Darcy law for pressure losses in channels.

$$\frac{\Delta p_{dh}}{\Delta p_{ch}} = \left(\frac{\dot{m}_{dh}}{\dot{m}_{ch}}\right)^2 \cdot \left(\frac{\rho_{ch}}{\rho_{dh}}\right) \tag{7}$$

Additionally, if the plant architecture with vapor bleeding from the turbine is considered (Fig. 4, right), the mass flow rate of the bleeding fraction (x_{bleed}) is computed considering the energy balance on the cold storage reported in Eq. (8).

$$\dot{Q}_{ch}^{cold} = \dot{Q}_{dh}^{cold} = \left[\dot{m}_{dh}(1 - x_{bleed})(h_8' - h_1') + \dot{m}_{dh}x_{bleed}(h_9' - h_1')\right] \tag{8}$$

4. Results and discussion

The results of the analysis in this work are obtained from more than 800 simulated cycles and are presented starting with the reference case, highlighting how the different choices on the design variables of the system impact the key performance indicators of the Carnot battery.

Afterwards, the implications of the variation of the same parameters are highlighted for different system configurations, as for various hot and cold storage technologies and different isentropic efficiencies of the turbomachinery in a wide range sensitivity analysis.

4.1. Reference case results

The reference case results are representative of a system with cold storage based on water/ice, and thus with a constant temperature of 0 °C, efficiency of turbomachinery equal to 85 % and 90 % for the compressor and the turbine respectively and Δp and Δ T as reported in Table 2. The optimal trend of the round-trip efficiency and energy density are discussed separately, presented only for the conditions at optimal charging and discharging cycle maximum pressure.

4.1.1. Round trip efficiency

The performances of the reference case system are reported in Fig. 11 as maps of RTE for both the chiller configuration and the system with vapor bleeding from the turbine. Each map comprises 49 cases obtained by optimizing the value of the temperature T_4 during the charging phase while still leaving p_{ch} and p_{dh} as the two main sensitivity variables. Contour plot of Fig. 11 reports the optimal value of T_4 for the two cases for each combination of charging and discharging maximum pressure.

The two cycle configurations present a similar RTE trend, with a high RTE region on the diagonal of the p_{ch}-p_{dh} heatmap. Moreover, the system employing vapor bleeding is generally more efficient compared to the case with a chiller. Three regions, highlighted in Fig. 11 (region **A**, **B** and **C**) are further analysed, to provide a better understanding of the obtained results.

Region **A** represents conditions at the RTE optimum for the minimum cycle charging pressure investigated in this work (i.e., 80 bar).For these cases, the optimal discharging maximum cycle pressure is larger (i.e. 125 bar) than the charging one and the turbine outlet condition is inside the saturation dome, so that the recuperator is bypassed in the discharging phase, as reported in Fig. 12.**b**.

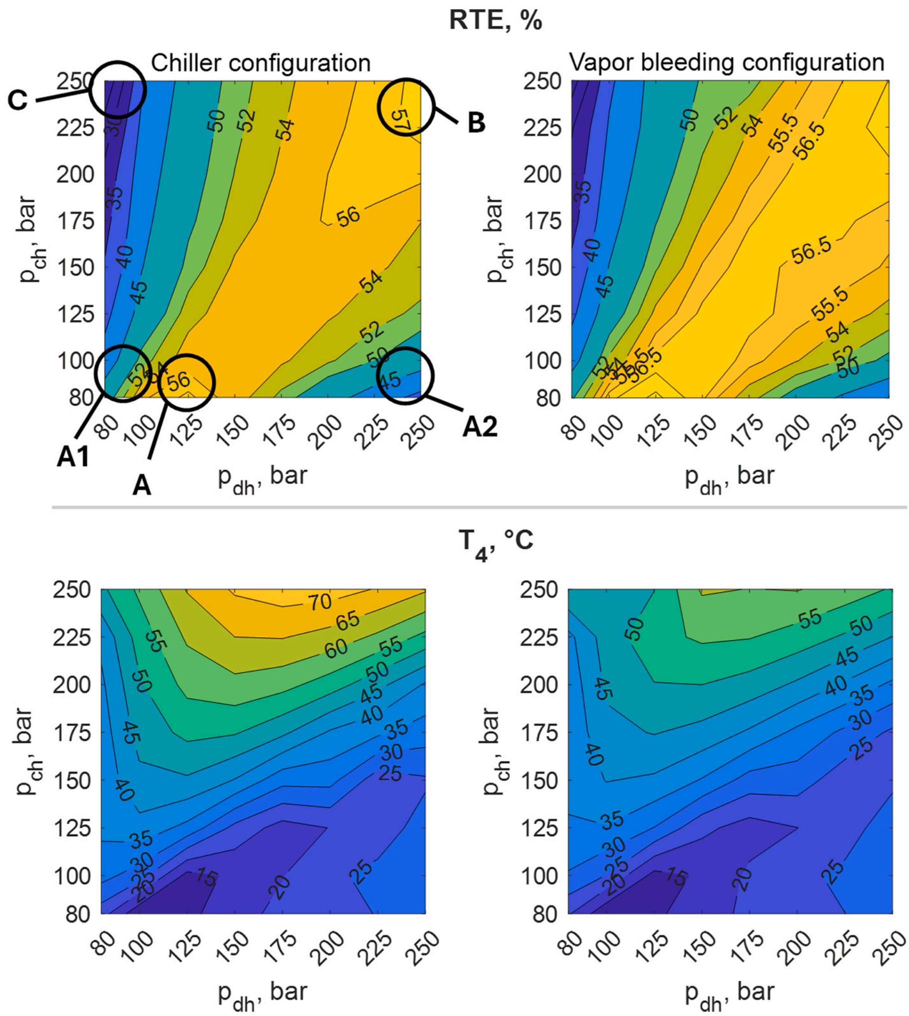

Fig. 11. Trend of the RTE and T_4 for the chiller (left) and vapor bleeding (right) configuration, with $T_{cold} = 0°C$.

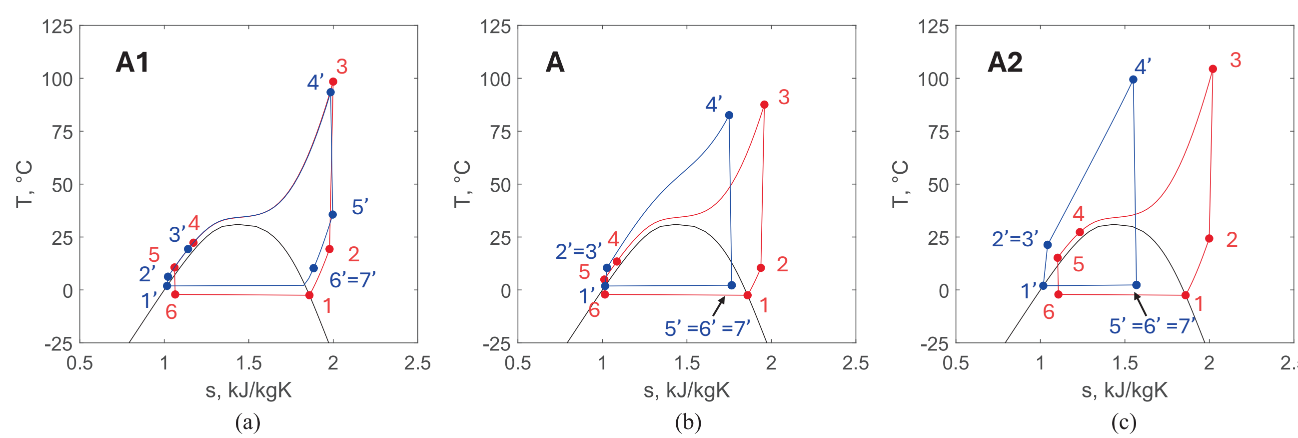

Fig. 12. Optimal points at$p_{ch} = 80$ bar, $T_{cold} = 0°C$ and different discharging pressure for the chiller configuration. Configuration at $p_{dh} = 80$ bar, representing region **A1** (a). At$p_{dh} = 125$ bar, representing region **A** (b). At$p_{dh} = 250$ bar, representing region **A2** (c).

For the same charging pressure (80 bar), a discharging pressure lower than the optimum would imply lower turbine expansion ratio, a lower electrical power production and a higher thermal power rejected to the cold storage thus penalizing the RTE (Fig. 12**.a** and region A1). Differently, cases with a discharging pressure higher than the optimum value (Fig. 12**.c** and region A2), show a lower RTE due to a larger increase of pump work than the turbine one. Furthermore, the much lower vapor quality at turbine outlet would also imply issues on last turbine stage performance and lifetime, although these effects are not accounted for in this work.

Even though the recuperator is bypassed during the discharging phase, its presence is beneficial in charging phase, as it allows to increase the compressor inlet temperature. On one hand, this increases the compressor work for a given expansion ratio, while, on the other hand, it

(i) raises the maximum temperature of the system and allows for a improved turbine power production during discharging phase and (ii) leads to a reduction in the enthalpy of the working fluid at the evaporator inlet, thus increasing the coefficient of performance (COP) of the heat pump in the charging phase.

Region **B** identifies optimal RTE configurations at maximum charging cycle pressure (i.e., 250 bar in his work) and very similar discharging cycle pressure. In this region the optimal solutions feature higher temperatures (close to 300 °C) thanks to the increased internal cycle recuperation and the higher pressure ratio, as reported in Fig. 13. The higher maximum temperature leads to an increase of the temperature difference between the cold and the hot storage, reducing the impact of the assumed PHE terminal ΔT and the evaporator/condenser pinch point ΔT on the RTE. Despite the benefits of an increased maximum temperature, the values of RTE are comparable with the ones of region **A,** due to the additional recuperator process and to the increase in the compressor consumption caused by the higher pressure ratio and inlet temperature. Moreover, the higher the maximum pressure, the greater the specific work and CO_2 density, leading to more compact exchangers and to turbomachinery with smaller cross-sectional area, and thus to a potentially lower cost of the equipment. On the other hand, higher pressures would also lead to a higher number of turbine and compressor stages and a more challenging design of system components, so the final choice of the design parameters requires a more detailed techno-economic analysis, which will be the focus of future studies.

Region **C** adopts $p_{ch} > p_{dh}$ and it is characterized by a low RTE mainly due to the poor efficiency of the discharging cycle, which works at low pressure ratio and thus achieves a lower expansion work and a large heat duty in the recuperator.

This aspect is evident comparing the results of region **B** and **C** (Fig. 13 and Fig. 14), where the charging phase is fixed (p_{ch} equal to 250 bar) and the discharging phase has similar turbine inlet temperature with very different turbine outlet temperature, due to the lower expansion ratio of region **C**. As the recuperator is designed for the charging phase, with a duty of 951 kW, the increase in the heat exchanged (by a factor of almost 3) requires a rise in the internal ΔT. Moreover, the lower value of p_{dh} increases the heat capacity of the CO_2 from point 2′ to 3′, as this heating process takes place closer to the critical point, leading to completely different temperature profiles inside the recuperator for the two phases. The consequence is a large irreversibility generation in the component during the discharging phase, which eventually leads to lower RTE compared to cases with higher discharging pressures.

Since the RTE of the Carnot battery is the product of the charging cycle COP and the discharging cycle thermal efficiency, Fig. 15 allows to better understand the trade-off related to each contribution. It is evident that, moving from region **A** to region **B**, the discharging phase performance increases at the expense of the COP. The reason is that the efficiency of power cycles improves with an increase in the difference between the maximum and minimum cycle temperatures, which is related to the temperature difference between the hot and cold storages, while the opposite is true for the heat pump process. The final effect is that the points that lie on the diagonal connecting region **A** and **B** have similar RTE (Fig. 11), as the increase in COP is almost proportional to the decrease in the cycle efficiency of the power cycle in the discharging phase ($\eta_{dh,Cycle}$).

Additionally, it is possible to notice that regions **B** and **C** show similar COPs, as the charging phase cycle does not significantly change in the two regions (Fig. 13, Fig. 14), while the lower discharge pressure level of region **C** highly penalizes the discharging phase efficiency compared to region **B** thus leading to the lower overall RTE, as already discussed. Both COP and $\eta_{dh,Cycle}$ are highly dependent on the value of p_{ch}, as it is directly connected to the cycles maximum temperatures, while the dependency on p_{dh} is less evident except in the region with $p_{ch} > p_{dh}$ where further lowering the discharging phase pressure level leads to large efficiency loss, as previously explained when analyzing region **C.**

The comparison between the chiller-based and the vapor bleeding-based configurations is reported in Fig. 16, where only the optimal points of the previous maps are reported. Both configurations present very similar trends of optimal discharging pressure level, with the value of p_{dh} always greater then p_{ch} except for cases of $p_{ch} > 225$ bar where the optimal discharging pressure level remains steady at 250 bar due to the imposed upper bound. This limitation leads to a flattening or even a decline in the RTE trend as the difference between the charging and discharging pressure level reduces.

The use of vapor bleeding instead of an external chiller leads to higher efficiencies, especially at lower charging pressure, with a RTE gain ranging from 0 % to 2 %, depending on the conditions. In the vapor bleeding configuration, the penalization related to the ambient condensation process is equivalent to the exergy loss caused by the direct heat released to the ambient: hence, the higher is the average bled vapor temperature and the amount of heat released, the higher is this penalization. Observing Fig. 17**.a** and Fig. 17**.b** it is evident that by increasing the charging pressure level p_{ch}, and consequently also the discharging one p_{dh}, the temperature of point 5′ increases too, thus increasing both the heat released to the ambient and the temperature at which this heat is released. The net effect is that the RTE improvement of the vapor bleeding solution becomes less relevant at higher pressures, as the bleeding penalization becomes more and more similar to the one related to the chiller consumption. It is also important to note that, for both configurations, the maximum RTE does not significantly change with the value of p_{ch}, consistently remaining within the range of 55 % to 58 %.

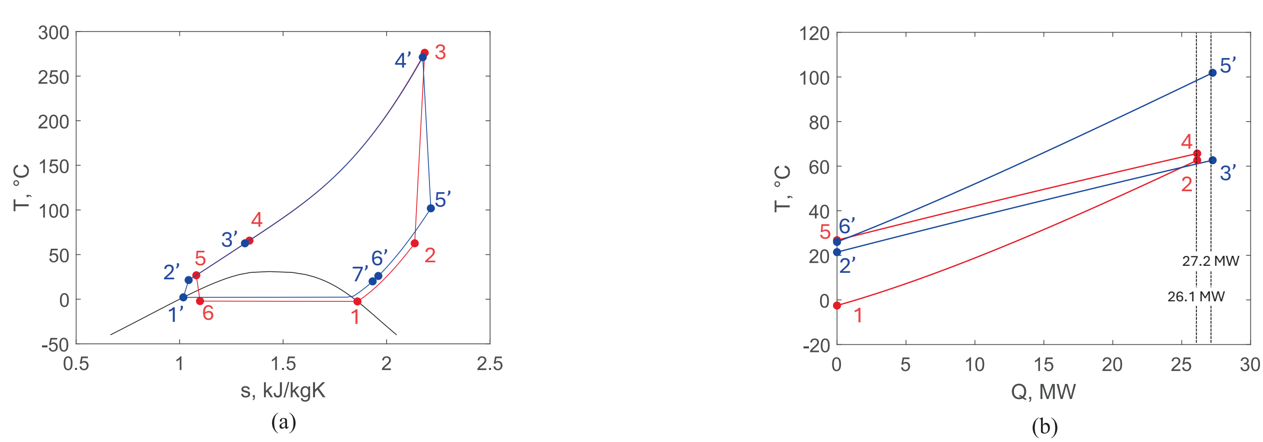

Fig. 13. T-s diagram of the optimal Carnot battery with $p_{ch} = 250$ bar, $p_{dh} = 250$ bar and $T_{cold} = 0°C$ for the chiller configuration, representing region **B** (a). Recuperator T-Q diagram of the charging and discharging phase for this optimal operating point (b).

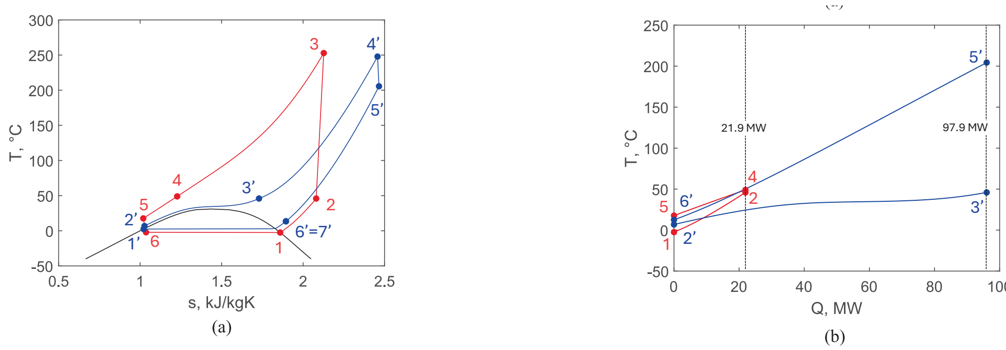

Fig. 14. T-s diagram of the optimal Carnot battery at p_{ch} = 250 bar, p_{dh}= 80 bar and T_{cold} = 0°C for the chiller configuration, representing region **C** (a). Recuperator T-Q diagram of the charging and discharging phase for this optimal operating point (b).

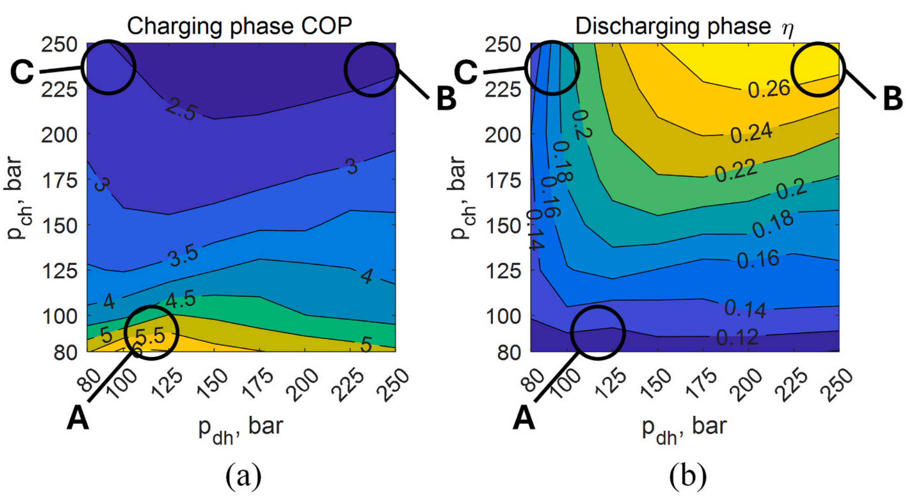

Fig. 15. Breakdown of the RTE into the COP (a) and $\eta_{dh,Cycle}$ (b) for the Carnot battery with the chiller configuration and T_{cold} = 0°C.

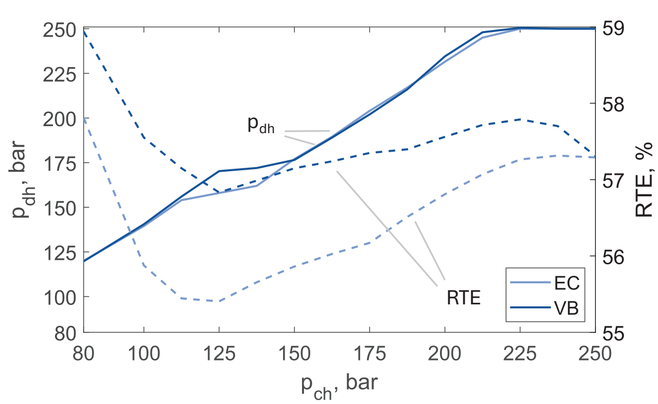

Fig. 16. Comparison of optimal RTE and p_{dh} for the chiller and the vapor bleeding-based configurations for T_{cold} = 0°C.

4.1.2. Energy density

While the variation of the pressure levels of the system has a limited impact on the RTE, a more pronounced effect is related to the energy density of the technology. Higher pressures allow for higher net specific work for both thermodynamic cycles, involving lower mass flow rates at fixed charging power consumption as visible in Fig. 18. More specifically, for the reference case (50 MW_{el}) moving from 80 bar to 250 bar cycle maximum pressure leads to a reduction of the working fluid flow rate from 1099 kg/s to 309 kg/s in the heat pump cycle and from 1360 kg/s and 311 kg/s in the power cycle. It must be noted that the obtained values are coherent with the ones found by *Echogen Power Systems* for their commercial scale plant design [76].

Additionally, increasing the pressure level in the charging phase reduces the heat released to the hot storage (shown in Fig. 19, left), as the COP of the charging phase is reduced (visible in Fig. 15, left), and increases the temperature span across the hot storage, since the maximum temperature of the charging cycle rises (on Fig. 19, right). Both effects lead to a reduction of the mass, and consequently of the volume, required by the hot storage (plotted in Fig. 20, left). Analogously, the cold storage volume is also reduced for higher charging pressures, as evident in Fig. 20, right.

The system pressures also affect the sizing of the turbomachinery. High operating pressures lead to smaller mass flow rates and higher CO_2 densities, allowing for smaller cross-sectional area for the turbomachinery. On the other hand, higher maximum pressures increase the turbine expansion ratio, increasing the number of stages needed. The impact on system size due to the variable dimensions of the turbomachinery has been neglected, being their volume negligeable with respect to hot and cold storage, while this aspect can affect techno-economic analyses that can be tackled in next steps of this study.

By combining the storage, the recuperator and the three container volumes (6 m x 3 m x 3 m), needed to accommodate the turbomachinery and the chiller, it is possible to obtain the overall volume of the system, and so its energy density, reported in Fig. 21. Moving from minimum (80 bar) to maximum (250 bar) charging pressure allows to increase the energy density by a factor equal to 5, leading to a lower system footprint and land occupation, as shown in the layouts depicted in Fig. 22. In particular, a drop from 60 $m^2/MWh_{el,dh}$ to 20 $m^2/MWh_{el,dh}$ is computed when moving from the low-pressure system (80 bar) to the high pressure one (250 bar). The plant scheme has been developed by choosing a

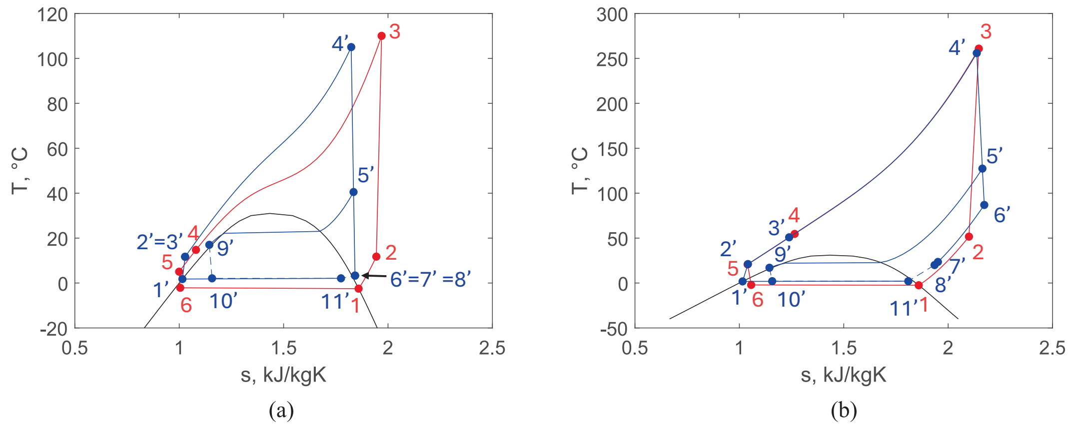

Fig. 17. Ts diagrams of the optimal CO_2 Carnot battery at T_{cold} = 0°C for the bleeding configuration. Condition withp_{ch} = 100 bar, p_{dh}= 140 bar representing region **A** (a). Condition withp_{ch} = 250 bar, p_{dh}= 250 bar representing region **B** (b).

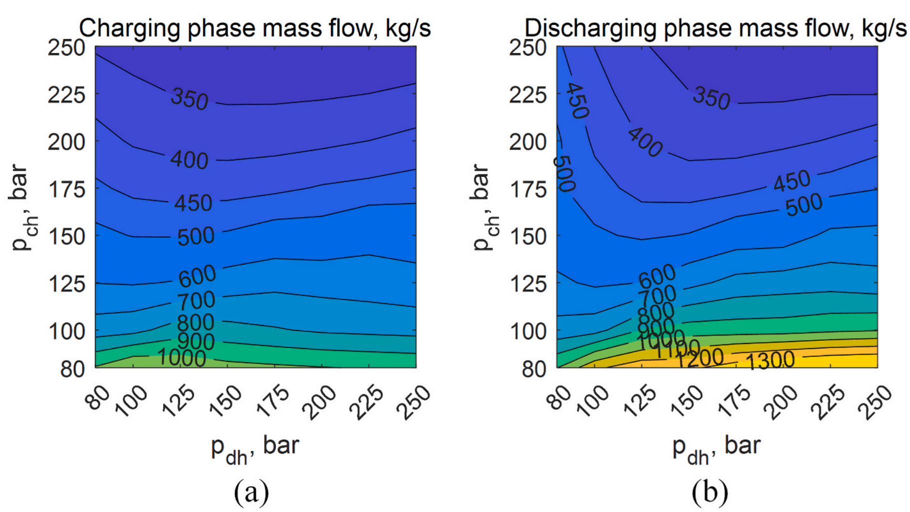

Fig. 18. Mass flow rate of the Carnot battery for a chiller-based configuration with T_{cold} = 0°C: charging phase (a), discharging phase (b).

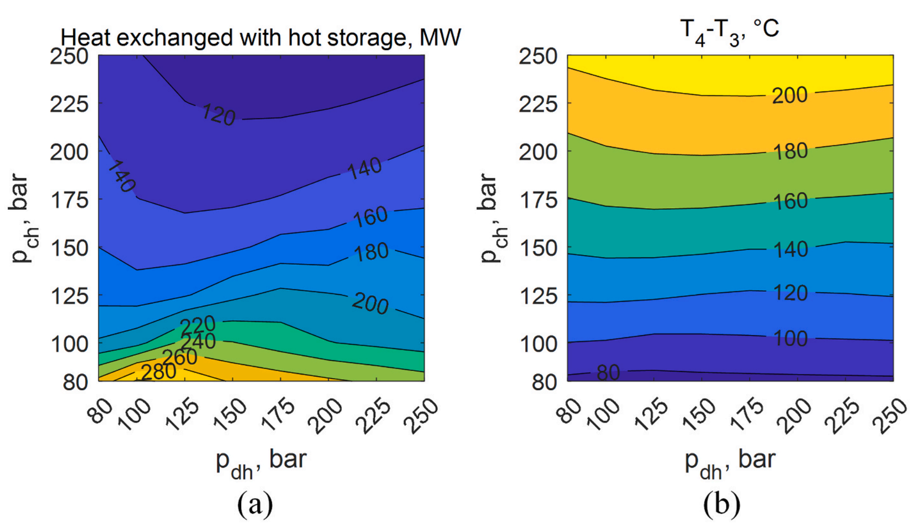

Fig. 19. Heat exchanged (a) and temperature span across the hot storage (b) for a chiller-based configuration with T_{cold} = 0°C.

similar layout and component aspect ratio as the one reported in the preliminary rendering by *Westinghouse Electric Company* [47] but further footprint reduction would be achievable by stacking differently the solid storage arrays.

Similar trends of energy density are computed for the vapor bleeding configuration: considering only the optimized condition of p_{dh}, the energy density of both configurations is shown in Fig. 23. The limited difference, slightly more marked at high maximum pressures, is due to

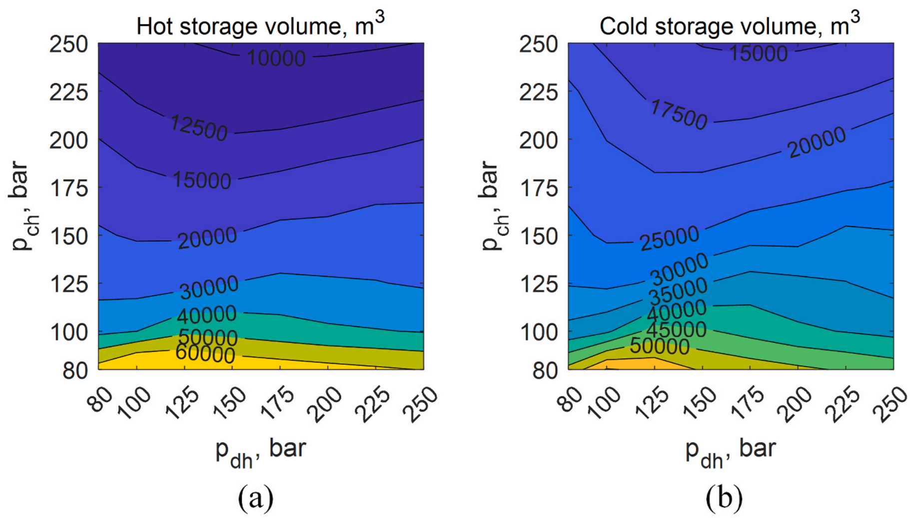

Fig. 20. Storage sizes for the chiller configuration with $T_{cold} = 0°C$: hot storage volume (a), cold storage volume (b).

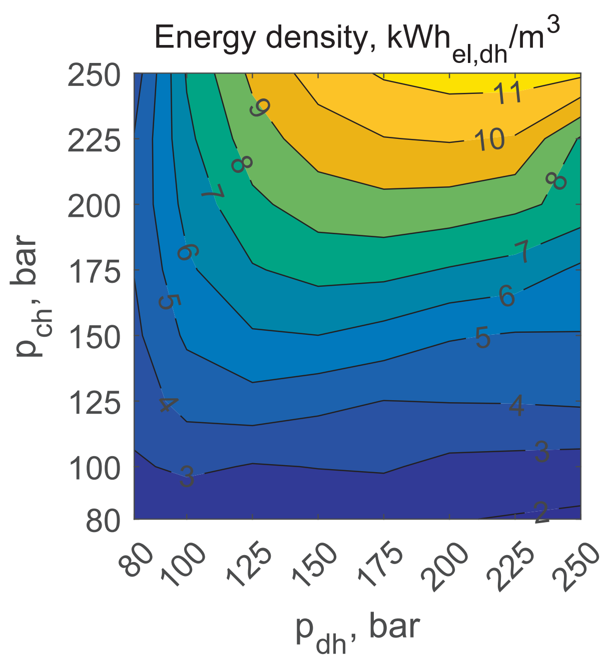

Fig. 21. Energy density for the chiller configuration with $T_{cold} = 0°C$.

the lower values of PHE outlet temperature in the charging phase (T_4). In fact, during the discharging phase, only a fraction of the CO_2 enters the recuperator on the hot side, leading to a less effective heat recovery and so to a lower value of the PHE inlet temperature ($T_{3'}$). The lower value of $T_{3'}$ brings to lower value of T_4, as they are linked by the hot storage terminal ΔT, and so to a lower charging phase maximum temperature (T_3), for the same p_{ch}.

This results in a higher COP of the charging phase compared to the chiller-based configuration, leading eventually to larger storage volumes as more energy is released to them. This effect is counter-balanced by the higher RTE of the vapor bleeding configuration. Nevertheless, since the RTE improvement of the vapor bleeding configuration reduces at higher pressures (Fig. 16), this solution becomes less energy dense compared to the one employing a chiller for highly pressurized systems.

Considering the resulting values, the configuration of Carnot battery proposed shows energy densities two orders of magnitude higher and system footprint one order of magnitude lower than CO_2 Battery systems, considering that the first commercial plant of *Energy Dome* is foreseen to have energy density of 0.17 kWh/m^3, with footprints of 235–250 m^2/MWh due to the large working fluid storage at ambient pressure [14].

4.2. Sensitivity analysis: Comparison with multi-tanks liquid storage

In this section, the benefits of the adopted solid medium storage system with respect to the multi-tank storage system is proposed as a function of the charging cycle maximum pressure.

The results for system with the chiller configuration are reported in Fig. 24: the multi-tank system has been simulated by assuming a storage with an infinite number of tanks, as the one reported in Fig. 7, by imposing a pinch point ΔT of 5 °C between the charging and discharging CO_2 temperature profiles, being thus representative of an ideal case with very large heat exchanger surfaces and high system complexity. It can be noted that for the multi-tank case the optimal p_{dh} is always very close, if not equal, to p_{ch}.

This difference with respect to the solid medium hot storage case, where the optimal region is characterized by $p_{dh} > p_{ch}$, is due to the need to match temperature profiles during both charging and discharging. The choice of the type of hot storage also impacts the overall trend of RTE, which is remarkably lower than the solid medium hot storage case, especially at low maximum pressures, as it can be seen in Fig. 24 and Fig. 25.

The penalization of the RTE compared to the solid storage case can be mitigated by employing high charging and discharging pressures, as the temperature profiles of CO_2 become more linear, thus reducing the temperature difference between the charging and discharging phases. However, increasing the pressure of the system also increases the maximum temperature of the working fluid and thus of the storage medium, requiring the use of high-pressure water, oils or molten salts as HTF that would lead to an increase in system cost and complexity. The maximum temperature of a pressurized water storage system is usually limited to 130–170 °C [35–37]. By respecting this limit the maximum RTE achievable is lowered to around 50 %, a value also confirmed in the literature [35].

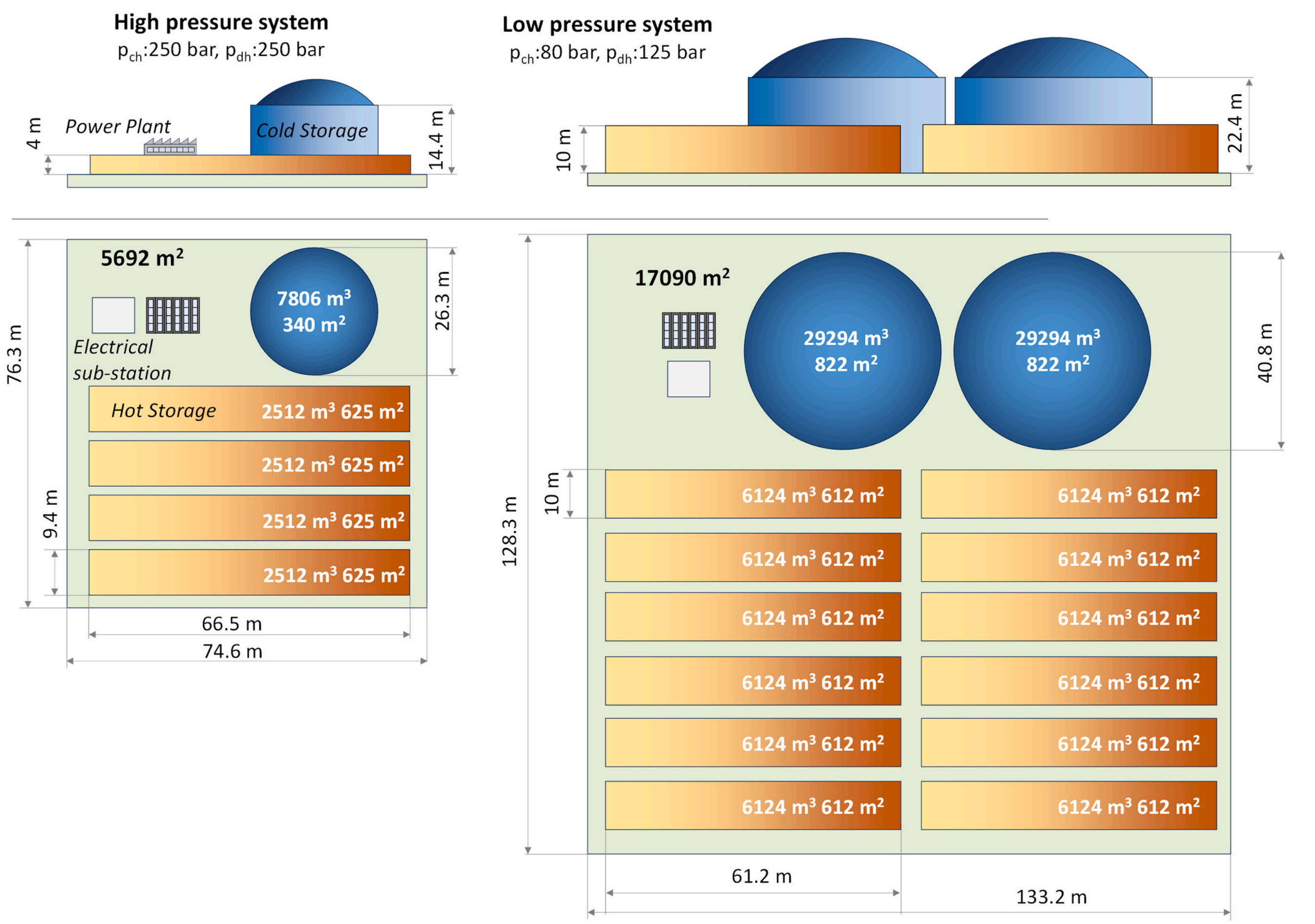

Fig. 22. Plant scheme and system footprint of the two solutions of Carnot battery with a power of $50MW_{el}$ and a 10 h storage: high pressure (left) and low pressure system (right).

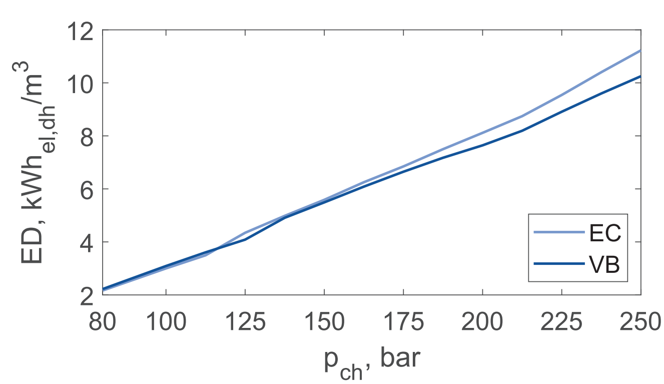

Fig. 23. Comparison between the energy density of the two configurations at $T_{cold} = 0°C$.

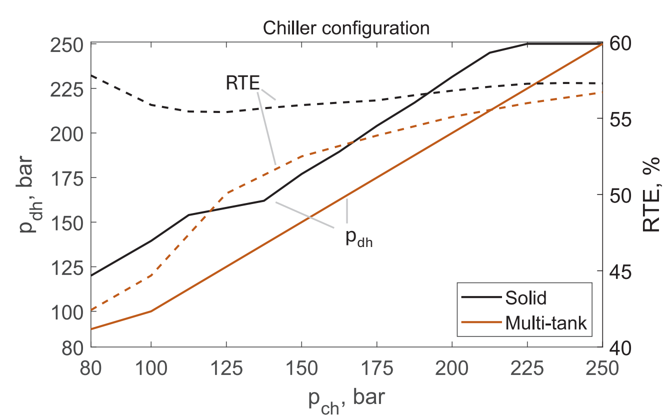

Fig. 24. Comparison of solid storage and multi-tank storage case for a chiller-based configuration

A final calculation is carried out for this latter case by adopting a 4-tanks storage system, rather than an ideal infinite number of HTF levels. Fig. 26 depicts the T-s diagram of the cycles for the optimal solution achievable under these conditions, with a maximum temperature of 150 °C of the pressurized water. The charging and discharging maximum pressures are thus fixed to 130 bar, computed to match the hot TES temperature levels and the computed RTE is 49.7 %, a value that represents only a net 0.8 % drop compared to case with infinite number of tanks (i.e. an ideal case) for the same maximum pressure. The T-Q diagram of the 4-tanks hot storage is reported in Fig. 27. For the simulations, the pinch point ΔT between the CO_2 and the storage thermal profile has been fixed to 2.5 °C in design conditions, to be consistent with the assumed pinch point ΔT for the ideal multi-tank case.

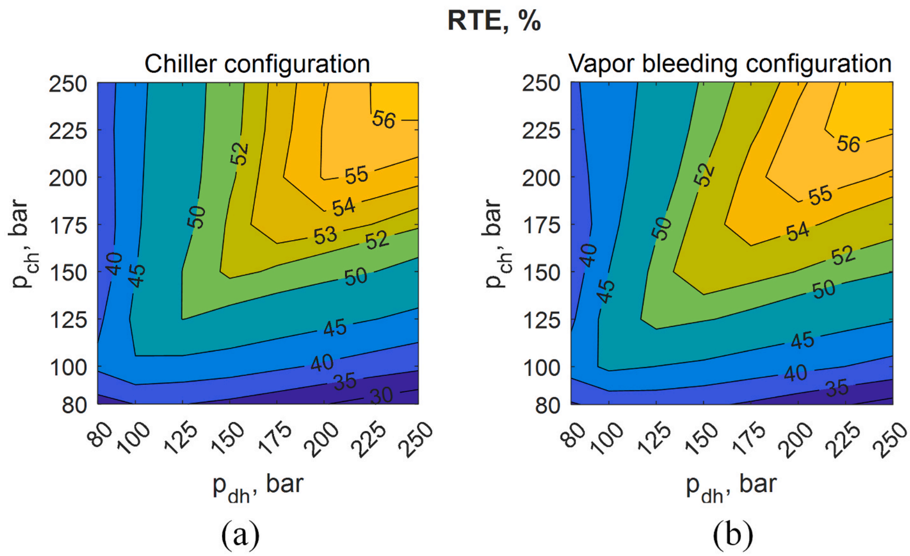

Fig. 25. Optimal RTE of the Carnot battery with $T_{cold} = 0°C$ for a solution with an ideal multi-tank liquid storage: Chiller based configuration (a), vapor bleeding configuration (b).

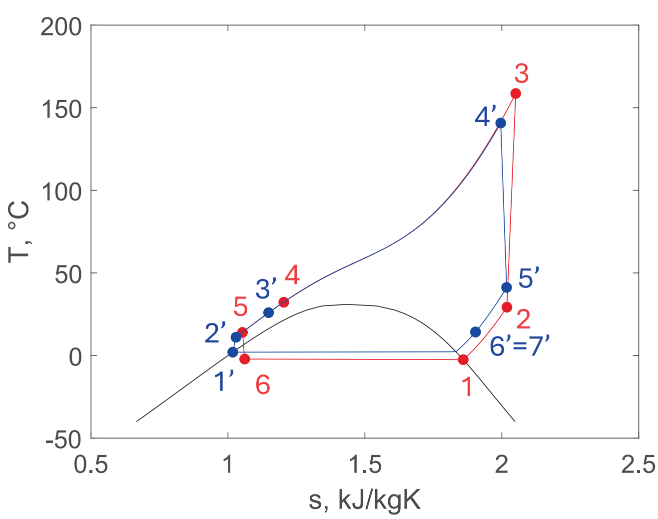

Fig. 26. T-s diagram of the optimal solution with a 4-tank water storage system ($T_{cold} = 0°C$, p_{ch}=p_{dh} = 130 bar).

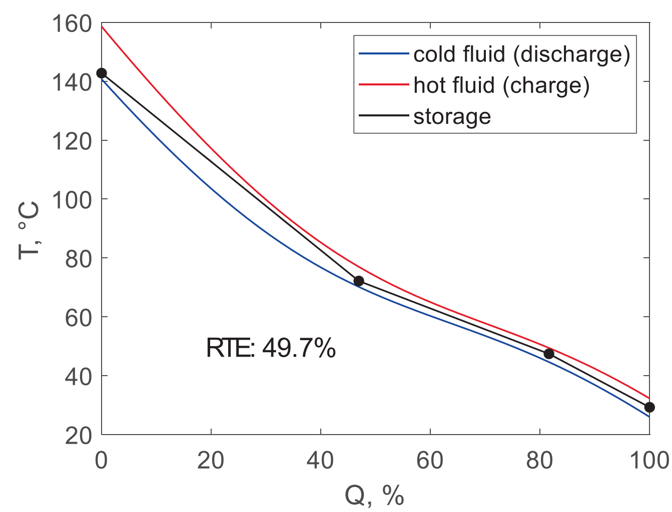

Fig. 27. Hot storage T-Q diagram of the optimal solution with a 4-tank water storage system ($T_{cold} = 0°C$, p_{ch}=p_{dh} = 130 bar).

4.3. Sensitivity analysis: Effect of the cold storage temperature

As the cold storage operates under cycling conditions, its temperature level can be considered a design parameter and, thanks to the availability of an adequate low temperature PCM, its temperature can be far below the ambient one, leading to an increase of the achievable RTE for all pressure levels.

For this reason, results analogous to the reference case are presented also with a cold storage temperature that is reduced to −30 °C. The trend of RTE is reported in Fig. 28, consistently with what can be already found in precedent literature works [36,37], showing a significant increment of the RTE when reducing the cold storage temperature. Additionally, the high RTE region shift even more toward the region where $p_{dh} > p_{ch}$, with the maximum RTE achieved for a charging pressure level of 80 bar, suggesting that even lower maximum pressures can be beneficial from performance perspective, penalizing the footprint and energy density of the system with respect to the simulations previously proposed.

In particular, considering the expander of the heat pump and the pump of the power cycle, reducing the cold storage temperature brings the working fluid at a lower reduced temperature during condensation (from around 0.9 to around 0.8), decreasing the work of both the expander and the pump. However, since the optimal region is characterized by discharging pressures greater than the charging ones, the benefit related to the reduction in the pump work is greater than the drawback of a reduction in expander work. Additionally, the decrease in the pump work leads to an increase in the difference between the turbine and the pump specific works, with higher optimal discharging phase pressure ratio and power cycle efficiency, even for configurations with low maximum temperature, thus increasing the RTE at lower p_{ch}.

With a cold storage temperature of −30 °C, the benefit in adopting the vapor bleeding configuration to ensure the energy balance at the cold storage is even more pronounced with respect to the case with the chiller, as the chiller EER decreases with respect to the 0 °C cold storage temperature case (from 8.19 to 2.43, assuming the same second law efficiency of the chiller), leading to an increase of system electrical self-consumption by a factor of 3.4. Accordingly, RTE higher than 65 % and 60 % can be obtained for the vapor bleeding and chiller cases, respectively. Moreover, lowering the cold storage temperature also increases the overall energy density, an effect that is a direct consequence of the

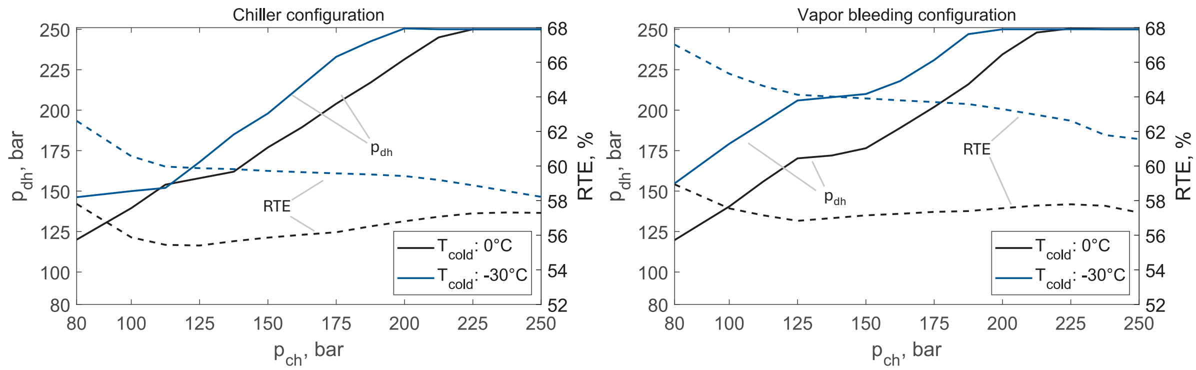

(a) (b)

Fig. 28. Effect on different T_{cold} on the performance of the Carnot battery for a chiller-based (a) and a vapor bleeding-based (b) configuration

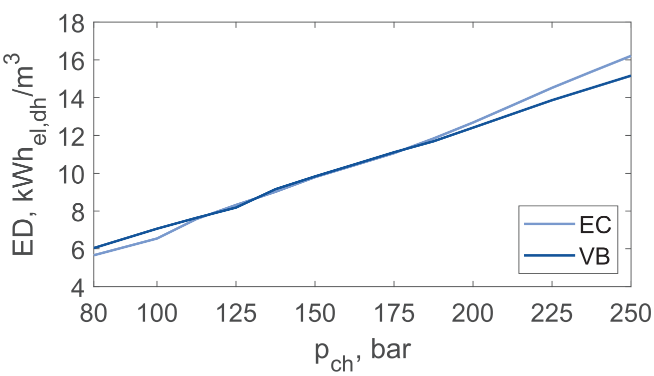

Fig. 29. Comparison between the energy density of the two configurations at T_{cold} = -30 °C.

increase in specific work and RTE.

For the chiller-based configuration the energy density increases up to 5.66 $kWh_{el,dh}/m^3$ for the low charging pressure cycle (80 bar) and up to 16.2 $kWh_{el,dh}/m^3$ for the high charging pressure system (250 bar) with an increase of around 162 % and 45 % with respect to the corresponding case at 0 °C, respectively. The energy density increment is more marked for low pressure systems, since their RTE increases is larger compared to high pressure system (Fig. 28). The same consideration applies also to systems employing vapor bleeding, and the comparison between the energy densities of the two solutions with T_{cold} = –30 °C is reported in Fig. 29.

Similarly to the case at T_{cold} = 0°C (referring to Fig. 23), the energy density is generally higher for the chiller-based configuration at high pressure level. Nevertheless, for T_{cold} = –30 °C the difference is smaller due to the much higher RTE of the other solution: in particular, for low pressure systems, the RTE improvement related to the heat rejection into the ambient is sufficiently high, making the vapor bleeding solution with an energy density slightly higher.

4.4. Sensitivity analysis: variation of the thermodynamic cycle main parameters

The previous analyses evidenced how the different design choices related to the whole Carnot battery system may influence its main KPI, focusing on the hot and cold storage. On the contrary, the following results investigate the impact of different assumptions on the cycle components selection and performances on the resulting RTE.

4.4.1. Sensitivity on PHE pressure drops and introduction of the throttling valve in the charging cycle

The impact of higher hot storage HX pressure drop at design conditions, from 1 % to 5 % (relative to the component inlet pressure in the charging cycle), negatively affects the system RTE: results are proposed for both the chiller-based system and the vapor bleeding-based system in Fig. 30. However, the RTE reduction is limited and always in the range of −2% to −3%. At the same time, the reduction of performance is way more significant (−5% in RTE) if the two-phase flow expander of the heat pump in the charging phase is replaced by a throttling valve.

This reduction in RTE can be attributed to two different effects penalizing the COP of the charging cycle: on one side, the use of a valve prevents to recover part of the compression work, on the other, due to the throttling process, the specific enthalpy of the CO_2 at the evaporator inlet is higher with respect to the case adopting an expander, thus lowering the heat exchanged with the cold storage during the evaporation process. This effect induces an increment of either the chiller

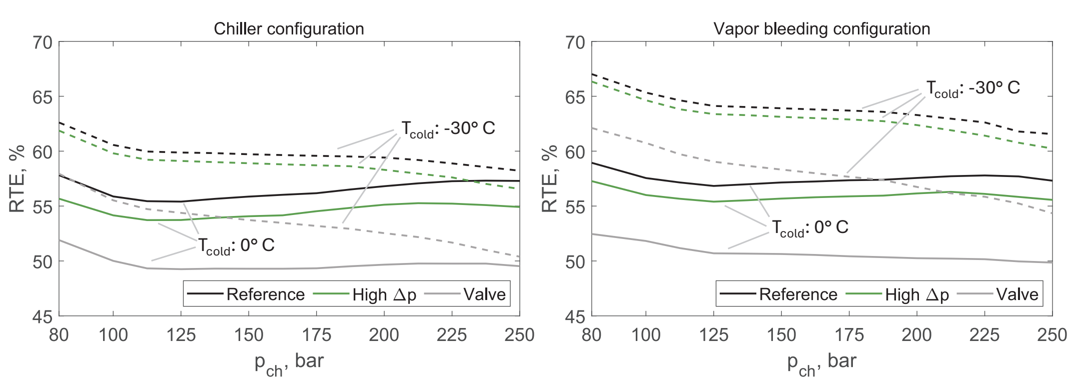

(a) (b)

Fig. 30. Effect of PHE Δp and employment of a valve on the RTE in the case of a chiller-based (a) and a vapor bleeding-based (b) configuration

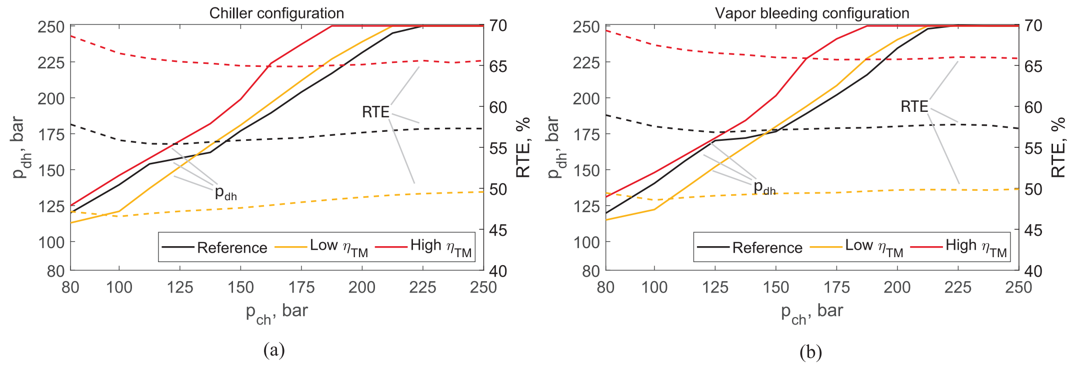

Fig. 31. Effect of turbomachinery efficiency on the RTE of the Carnot battery for the chiller-based configuration (a) and for the vapor bleeding configuration (b).

electric consumption or the fraction of vapor bled from the turbine, depending on the configuration adopted, further penalizing the efficiency.

The effect is more relevant for high p_{ch} and high T_{cold}, since at higher maximum pressures the turbine/valve pressure difference available increases, amplifying those effects. Differently, by lowering the cold storage temperature, thus throttling the fluid farther from the critical point, the valve Δp and the density of the fluid increase, lowering the impact of the throttling process on the overall RTE.

The trend of the optimal p_{dh} curves were not reported in this case as they coincide to the ones for the same cold storage temperature. In fact, introducing a penalization in pressure drop offsets the RTE of the vapor bleeding-based configuration as much as the one with a chiller, whereas the inclusion of a valve has a bigger penalizing effect on the chiller-based configuration, especially at T_{cold} = - 30 °C, due to its high specific consumption.

4.4.2. Sensitivity on turbomachinery efficiency

The effect of a variation in isentropic efficiency of the turbomachinery is investigated by varying the value of each turbomachinery efficiency by ± 5 percentage points compared to the reference values. The analysis performed aims at investigating different ranges of isentropic efficiencies that can be representative of: i) different sizes of the Carnot battery (either at the kW_{el}-scale or in the range of 50-100MW_{el}), ii) different turbomachinery technological readiness levels and manufacturing processes, representative of various maturity levels of CO_2-based technology.

The results of the RTE under these assumptions are shown in Fig. 31: it is possible to conclude that the adoption of high efficiency turbomachinery is fundamental to achieving remarkable RTE values, overcoming 65 % for the configurations proposed in this work. An interesting finding is that systems with high turbomachinery efficiency allow to achieve higher RTE at low p_{ch} and high p_{dh}, while higher pressure levels are needed to achieve the maximum RTE when the efficiencies of the turbomachinery are lower. In fact, as previously mentioned, in low-pressure systems (with $p_{dh} > p_{ch}$) all the temperature difference between the hot and cold storage is exploited during the discharging phase by the turbine expansion. As a result, the RTE of these systems is highly dependent on the difference between the specific works of the turbine and the pump, which strongly depends on the turbomachinery efficiencies.

5. Conclusions

In this work, the modelling of CO_2 PTES system has been analysed with the aim of quantify the impact on the RTE and the energy density under different plant design assumptions and operating parameters: accordingly, the results provide details about the suggested strategies in the optimization of such systems.

The system investigated differs from previous works for two key modelling choices that can positively affect the cost and reduce the complexity of the Carnot battery: firstly, the hot storage system is based on solids, decoupling the maximum charging and discharging pressure, secondly, the same heat exchangers (recuperator, condenser/evaporator and PHE) are adopted for both the charging and discharging processes, designed during the definition of the charging process and operated in off-design during the discharging process. More than 800 combinations of configurations have been optimized in terms of charging and discharging cycle maximum pressures and recuperator sizing, considering two different cycle configurations. Furthermore, a comprehensive sensitivity analysis has been carried out detailing the impact of the assumptions on cold storage temperature, pressure drops, turbomachinery efficiency, as well as the substitution of the two-phase flow expander with a throttling valve.

Considering a reference case of Carnot battery with cold storage at 0 °C, RTE around 57 % can be achieved, with a proper choice of maximum pressures of the two cycles. The energy density is maximized when the maximum pressures are maximized, with values up to 11 kWh_{el}/m^3. Additionally, lowering the temperature of the cold storage boost both the energy density and the RTE, while comparing the Carnot battery with solids to a multi-tank configuration for the hot storage, it is showed that the solid based solution is favourable in terms of RTE, validating the interest on the proposed solution.

Finally, the influence of turbomachinery efficiencies, pressure drops and the use of a throttling valve instead of an expander were investigated. While higher pressure drops in the hot storage heat exchanger do not significantly affect the RTE, the other two aspects greatly influence the performance: for example, the use of the throttling valve the charging phase reduces the maximum RTE by around 5 % to 10 %, with a less marked penalization for cases at lower T_{cold} and for cases employing vapor bleeding.

This study demonstrates that the proposed system can achieve a round-trip efficiency around 57 % adopting conventional components, a value that can be pushed up to around 70 % if high performance turbomachinery is adopted or PCM for cold storage temperatures below 0 °C are selected. This level of performance makes this technology competitive with other thermomechanical energy storage technologies such as LAES (characterized by RTE of around 55 % [77]), A-CAES (at 65 % RTE) [78] and with the CO_2 Battery at 75 % [14], without their geological and practical limitations.

Moreover, it shows energy densities two orders of magnitude higher and system footprint one order of magnitude lower than CO_2 Battery systems.

Possible further developments of this study include a techno-economic analysis to assess the economic viability and the technology readiness: the investigation of different charging and discharging profiles, with a particular focus on off-design operation, would provide valuable insights into the system flexibility. Finally, future works could focus on feasibility studies related to specific case studies where the availability of heat, cooling and electrical production can unlock synergies from a sector coupling perspective.

CRediT authorship contribution statement

Simone Girelli: Conceptualization, Data curation, Formal analysis, Investigation, Methodology, Software, Visualization, Writing – original draft, Writing – review & editing. **Dario Alfani:** Conceptualization, Formal analysis, Investigation, Methodology, Software, Writing – original draft, Writing – review & editing. **Ettore Morosini:** Conceptualization, Formal analysis, Investigation, Methodology, Writing – original draft, Writing – review & editing. **Marco Astolfi:** Conceptualization, Formal analysis, Investigation, Methodology, Visualization, Supervision, Writing – original draft, Writing – review & editing.

Declaration of competing interest

The authors declare the following financial interests/personal relationships which may be considered as potential competing interests: Dario Alfani reports financial support was provided by NEST – Network 4 Energy Sustainable Transition. Ettore Morosini reports financial support was provided by MUR Progetti di Rilevante Interesse Nazionale. If there are other authors, they declare that they have no known competing financial interests or personal relationships that could have appeared to influence the work reported in this paper.

Acknowledgments

This study was carried out within the NEST - Network 4 Energy Sustainable Transition (D.D. 1243 02/08/2022, PE00000021) and received funding under the National Recovery and Resilience Plan (NRRP), Mission 4 Component 2 Investment 1.3, funded from the European Union - NextGenerationEU. This manuscript reflects only the authors' views and opinions, neither the European Union nor the European Commission can be considered responsible for them.

This paper is part of the project HICLOPS "High-medium temperature closed power cycles for waste heat recovery and renewable sources" that has received funding from the MUR Progetti di Rilevante Interesse Nazionale (PRIN) Bando 2022 under grant No 2022HMZ39A.

Data availability

No data was used for the research described in the article.

References

[1] Twitchell J, DeSomber K, Bhatnagar D. Defining long duration energy storage. J Storage Mater 2023;60. https://doi.org/10.1016/j.est.2022.105787.
[2] 'Carbon intensity of electricity generation', Our World in Data. Accessed: Feb. 13, 2025. [Online]. Available: https://ourworldindata.org/grapher/carbon-intensity-electricity?tab=chart&country=EU-27~OWID_EU27~CHN~USA.
[3] 'Home | California ISO'. Accessed: Sep. 06, 2024. [Online]. Available: https://www.caiso.com/.
[4] Bird L, et al. Wind and solar energy curtailment: a review of international experience. Renew Sustain Energy Rev 2016;65:577–86. https://doi.org/10.1016/j.rser.2016.06.082.
[5] Denholm P, Mai T. Timescales of energy storage needed for reducing renewable energy curtailment. Renew Energy 2019;130:388–99. https://doi.org/10.1016/j.renene.2018.06.079.
[6] Golden R, Paulos B. Curtailment of renewable energy in California and beyond. Electr J 2015;28(6):36–50. https://doi.org/10.1016/j.tej.2015.06.008.
[7] Rahman MM, Oni AO, Gemechu E, Kumar A. Assessment of energy storage technologies: a review. Energ Conver Manage 2020;223. https://doi.org/10.1016/j.enconman.2020.113295.
[8] Nogueira R, Flores AT, Perrella A. Pumped hydro storage plants: a review', Journal of the Brazilian Society of Mechanical Sciences and Engineering, vol. 42, no. 8, 2020, doi: 10.1007/s40430-020-02505-0.
[9] Schimpe M, et al. Energy efficiency evaluation of a stationary lithium-ion battery container storage system via electro-thermal modeling and detailed component analysis. Appl Energy 2018;210:211–29. https://doi.org/10.1016/j.apenergy.2017.10.129.
[10] Huber ST, Steininger KW. Critical sustainability issues in the production of wind and solar electricity generation as well as storage facilities and possible solutions. J Clean Prod 2022;339. https://doi.org/10.1016/j.jclepro.2022.130720.
[11] Budt M, Wolf D, Span R, Yan J. A review on compressed air energy storage: basic principles, past milestones and recent developments. Appl Energy 2016;170:250–68. https://doi.org/10.1016/j.apenergy.2016.02.108.
[12] Hydrostor, 'Willow Rock Energy Storage Center', Hydrostor.ca. Accessed: Jan. 01, 2024. [Online]. Available: https://hydrostor.ca/projects/willow-rock-energy-storage-center/.
[13] Highview Power, 'Ongoing Projects', highviewpower.com. Accessed: Jan. 01, 2024. [Online]. Available: https://highviewpower.com/projects/#uk-projects.
[14] Astolfi M, Rizzi D, Macchi E, Spadacini C. A novel energy storage system based on carbon dioxide unique thermodynamic properties. J Eng Gas Turbines Power 2022;144(8). https://doi.org/10.1115/1.4054750.
[15] Dumont O, Frate GF, Pillai A, Lecompte S, De Paepe M, Lemort V. Carnot battery technology: a state-of-the-art review. J Storage Mater 2020;32. https://doi.org/10.1016/j.est.2020.101756.
[16] Xia R, et al. Comprehensive performance analysis of cold storage Rankine Carnot batteries: energy, exergy, economic, and environmental perspectives. Energ Conver Manage 2023;293. https://doi.org/10.1016/j.enconman.2023.117485.
[17] Scharrer D, Bazan P, Pruckner M, German R. Simulation and analysis of a Carnot Battery consisting of a reversible heat pump/organic Rankine cycle for a domestic application in a community with varying number of houses. Energy 2022;261. https://doi.org/10.1016/j.energy.2022.125166.
[18] Poletto C, Dumont O, De Pascale A, Lemort V, Ottaviano S, Thomé O. Control strategy and performance of a small-size thermally integrated Carnot battery based on a Rankine cycle and combined with district heating. Energ Conver Manage 2024;302. https://doi.org/10.1016/j.enconman.2024.118111.
[19] Zhang X, et al. The Carnot batteries thermally assisted by the steam extracted from thermal power plants: a thermodynamic analysis and performance evaluation. Energ Conver Manage 2023;297. https://doi.org/10.1016/j.enconman.2023.117724.
[20] Zhang M, et al. Configuration mapping of thermally integrated pumped thermal energy storage system. Energ Conver Manage 2023;294. https://doi.org/10.1016/j.enconman.2023.117561.
[21] Morosini E, Alfani D, Renzoni M, Manzolini G. Thermally integrated innovative Carnot batteries to upgrade and dispatch low temperature sensible waste heat. J Phys Conf Ser 2024;2893(1):Nov. https://doi.org/10.1088/1742-6596/2893/1/012056.
[22] Malta Inc., 'Our Solution | Malta', maltainc.com. Accessed: Jan. 01, 2024. [Online]. Available: https://www.maltainc.com/solution/.
[23] McTigue JD, Farres-Antunez P, Markides CN, White AJ. Techno-economic analysis of recuperated Joule-Brayton pumped thermal energy storage. Energ Conver Manage 2022;252:Jan. https://doi.org/10.1016/j.enconman.2021.115016.
[24] 'RESTORE H2020 project'. Accessed: Feb. 13, 2025. [Online]. Available: https://www.restore-dhc.eu/.
[25] 'CHESTER H2020 Project'. Accessed: Feb. 13, 2025. [Online]. Available: https://www.chester-project.eu/.
[26] 'SEHERENE Project'. Accessed: Feb. 13, 2025. [Online]. Available: https://sehrene.eu/.
[27] 'Supercritical Transformational Electric Power (STEP) Project', Sandia National Laboratories. Accessed: Feb. 13, 2025. [Online]. Available: https://www.sandia.gov/energy/programs/nuclear-energy/advanced-energy-conversion/supercritical-transformational-electric-power-step-nuclear-energy/.
[28] 'sCO2-flex', sCO2flex. Accessed: Feb. 13, 2025. [Online]. Available: https://www.sco2-flex.eu/.
[29] Alfani D, Neises T, Astolfi M, Binotti M, Silva P. Techno-economic analysis of CSP incorporating sCO2 brayton power cycles: trade-off between cost and performance, presented at the SOLARPACES 2020: 26th International Conference on Concentrating Solar Power and Chemical Energy Systems, Freiburg, Germany, 2022. doi: 10.1063/5.0086353.
[30] Alfani D, Binotti M, Macchi E, Silva P, Astolfi M. sCO2 power plants for waste heat recovery: design optimization and part-load operation strategies. Appl Therm Eng 2021;195. https://doi.org/10.1016/j.applthermaleng.2021.117013.
[31] Chan W, Morosuk T, Li X, Li H. Allam cycle: Review of research and development. Energ Conver Manage 2023;294. https://doi.org/10.1016/j.enconman.2023.117607.
[32] Zelaschi A, Giostri A, Chiesa P, Martelli E. Semi-closed oxy-combustion combined cycles for combined heat and power applications, Journal of Engineering for Gas Turbines and Power, vol. 147, no. 4, Apr. 2025, doi: 10.1115/1.4066424.
[33] Chen D, Han Z, Han X, Li P. Design, operation, and case analyses of a novel thermodynamic system combining coal-fired cogeneration and decoupled Carnot battery using CO2 as working fluid. Energ Conver Manage 2023;296. https://doi.org/10.1016/j.enconman.2023.117680.

[34] Wang K, Shi X, He Q. Thermodynamic analysis of novel carbon dioxide pumped-thermal energy storage system. Appl Therm Eng 2024;255. https://doi.org/10.1016/j.applthermaleng.2024.123969.
[35] Mercangöz M, Hemrle J, Kaufmann L, Z'Graggen A, Ohler C. Electrothermal energy storage with transcritical CO 2 cycles. Energy 2012;45(1):407–15. https://doi.org/10.1016/j.energy.2012.03.013.
[36] Morandin M, Maréchal F, Mercangöz M, Buchter F. Conceptual design of a thermo-electrical energy storage system based on heat integration of thermodynamic cycles – part A: methodology and base case. Energy 2012;45(1):375–85. https://doi.org/10.1016/j.energy.2012.03.031.
[37] Morandin M, Maréchal F, Mercangöz M, Buchter F. Conceptual design of a thermo-electrical energy storage system based on heat integration of thermodynamic cycles – part B: alternative system configurations. Energy 2012;45(1):386–96. https://doi.org/10.1016/j.energy.2012.03.033.
[38] Ayachi F, Tauveron N, Tartière T, Colasson S, Nguyen D. Thermo-electric energy storage involving CO2 transcritical cycles and ground heat storage. Appl Therm Eng 2016;108:1418–28. https://doi.org/10.1016/j.applthermaleng.2016.07.063.
[39] Kim Y-M, Shin D-G, Lee S-Y, Favrat D. Isothermal transcritical CO2 cycles with TES (thermal energy storage) for electricity storage. Energy 2013;49:484–501. https://doi.org/10.1016/j.energy.2012.09.057.
[40] 'Electro-thermal Energy Storage (MAN ETES)', MAN Energy Solutions. Accessed: Jan. 01, 2023. [Online]. Available: https://www.man-es.com/energy-storage/solutions/energy-storage/electro-thermal-energy-storage.
[41] Wolscht L, Knobloch K, Jacquemoud E, Jenny P. Dynamic Simulation and Experimental Validation of a 35 MW Heat Pump Based on a Transcritical CO2 Cycle, Conference Proceedings of the European sCO2 Conference5th European sCO2 Conference for Energy Systems: March 14-16, vol. 2023, p. 93, Apr. 2023, doi: 10.17185/DUEPUBLICO/77273.
[42] 'ETES System Overview | Echogen Power Systems', www.echogen.com. Accessed: Jan. 01, 2023. [Online]. Available: https://www.echogen.com/energy-storage/etes-system-overview/.
[43] Hoppe J. Press Release MAN and ABB Introduce Unique Energy Storage Solution, Jun. 2018. Accessed: Jan. 01, 2023. [Online]. Available: https://www.man-es.com/docs/default-source/press-releases-new/180626-man-press-release_etes_en.pdf?sfvrsn=d169f4a1_2.
[44] Hemrle J, Kaufmann L, Mercangoez M. Thermoelectric Energy Storage System Having Two Thermal Baths and Method for Storing Thermoelectric Energy. Accessed: Jan. 01, 2023. [Online]. Available: https://patents.google.com/patent/US8584463B2/en.
[45] Hemrle J, Kaufmann L, Mercangoez M. Thermoelectric Energy Storage System with an Intermediate Storage Tank and Method for Storing Thermoelectric Energy. Accessed: Jan. 01, 2023. [Online]. Available: https://patents.google.com/patent/US8904793B2/en.
[46] 'MAN Esbjerg Heat Pump', MAN Energy Solutions. Accessed: Feb. 13, 2025. [Online]. Available: https://www.man-es.com/company/press-releases/press-details/2024/11/28/mega-heat-pump-delivers-first-heat-in-esbjerg.
[47] Westinghouse Electric Company, 'Westinghouse LDES', westinghousenuclear.com. Accessed: Jan. 01, 2024. [Online]. Available: https://info.westinghousenuclear.com/news/westinghouse-long-duration-energy-storage-solution-selected-for-department-of-energy-program-in-alaska.
[48] Held TJ, Miller J, Mallinak J, Avadhanula V, Magyar L. Pilot-Scale Testing of a Transcritical CO2-Based Pumped Thermal Energy Storage (PTES) System, in Volume 6: Education; Electric Power; Energy Storage; Fans and Blowers, London, United Kingdom: American Society of Mechanical Engineers, Jun. 2024. doi: 10.1115/GT2024-129211.
[49] Wang Y, Xie G, Zhu H, Yuan H. Assessment on energy and exergy of combined supercritical CO2 Brayton cycles with sizing printed-circuit-heat-exchangers. Energy 2023;263. https://doi.org/10.1016/j.energy.2022.125559.
[50] Sanz Garcia L, Jacquemoud E, Jenny P. Thermo-economic heat exchanger optimization for Electro-Thermal Energy Storage based on transcritical CO2 cycles, Conference Proceedings of the European sCO2 Conference3rd European Conference on Supercritical CO2 (sCO2) Power Systems 2019: 19th-20th September 2019, p. 353, Oct. 2019, doi: 10.17185/DUEPUBLICO/48917.
[51] Alva G, Lin Y, Fang G. An overview of thermal energy storage systems. Energy 2018;144:341–78. https://doi.org/10.1016/j.energy.2017.12.037.
[52] Tawalbeh M, Khan HA, Al-Othman A, Almomani F, Ajith S. A comprehensive review on the recent advances in materials for thermal energy storage applications. Int J Thermof 2023;18. https://doi.org/10.1016/j.ijft.2023.100326.
[53] Wu M, Li M, Xu C, He Y, Tao W. The impact of concrete structure on the thermal performance of the dual-media thermocline thermal storage tank using concrete as the solid medium. Appl Energy 2014;113:1363–71. https://doi.org/10.1016/j.apenergy.2013.08.044.
[54] Xu B, Han J, Kumar A, Li P, Yang Y. Thermal storage using sand saturated by thermal-conductive fluid and comparison with the use of concrete. J Storage Mater 2017;13:85–95. https://doi.org/10.1016/j.est.2017.06.010.
[55] Mitali J, Dhinakaran S, Mohamad AA. Energy storage systems: a review. Energy Storage Sav 2022;1(3):166–216. https://doi.org/10.1016/j.enss.2022.07.002.
[56] Sharma A, Tyagi VV, Chen CR, Buddhi D. Review on thermal energy storage with phase change materials and applications. Renew Sustain Energy Rev 2009;13(2):318–45. https://doi.org/10.1016/j.rser.2007.10.005.
[57] Agyenim F, Hewitt N, Eames P, Smyth M. A review of materials, heat transfer and phase change problem formulation for latent heat thermal energy storage systems (LHTESS). Renew Sustain Energy Rev 2010;14(2):615–28. https://doi.org/10.1016/j.rser.2009.10.015.
[58] Yang L, et al. A comprehensive review on sub-zero temperature cold thermal energy storage materials, technologies, and applications: state of the art and recent developments. Appl Energy 2021;288. https://doi.org/10.1016/j.apenergy.2021.116555.
[59] Thermofin, 'CRISTOPIA : Thermal energy storage solution', thermofin.net. Accessed: Jan. 01, 2024. [Online]. Available: https://thermofin.net/products/cristopia-thermal-energy-storage/.
[60] Weiland N, Thimsen D. A Practical Look at Assumptions and Constraints for Steady State Modeling of sCO2 Brayton Power Cycles, presented at the The 5th International sCO2 Power Cycles Symposium, Mar. 2016. Accessed: Mar. 15, 2025. [Online]. Available: https://www.osti.gov/biblio/1491086.
[61] Garcia LS, Jacquemoud E, Jenny P. Large Scale Tri-Generation Energy Storage System for Heat, Cold and Electricity based on Transcritical CO2 Cycles. presented at the The 7th International sCO2 Power Cycles Symposium. 2022.
[62] Span R, Wagner W. A new equation of state for carbon dioxide covering the fluid region from the triple-point temperature to 1100 K at pressures up to 800 MPa. J Phys Chem Ref Data 1996;25(6):1509–96. https://doi.org/10.1063/1.555991.
[63] Alfani D, Astolfi M, Binotti M, Silva P. Part-load strategy definition and preliminary annual simulation for small size sCO2-based pulverized coal power plant. J Eng Gas Turbines Power 2021;143(9):Sep. https://doi.org/10.1115/1.4051003.
[64] MATLAB, 'Global Optimization Toolbox User's Guide', Sep. 2024, Accessed: Feb. 25, 2025. [Online]. Available: https://www.mathworks.com/help/pdf_doc/gads/gads.pdf.
[65] Thu SM, Win TZ, Kyi HLT. A study on COP of existing ice plant. Int J Sci Eng Appl 2019;8:348–52.
[66] Bu XB, Li HS, Wang LB. Performance analysis and working fluids selection of solar powered organic Rankine-vapor compression ice maker. Sol Energy 2013;95:271–8. https://doi.org/10.1016/j.solener.2013.06.024.
[67] Expósito A, Payá IG, Pérez BP, de la Flor FJS, Lissén JMS. Experimental performance analysis of a novel ultra-low charge ammonia air condensed chiller. Appl Therm Eng 2021;195. https://doi.org/10.1016/j.applthermaleng.2021.117117.
[68] Gnielinski V. New equations for heat and mass transfer in turbulent pipe and channel flow. Int Chem Eng 1976;16(2):359–68.
[69] Chen NH. An explicit equation for friction factor in pipe. Indus Eng Chem Fundamentals 1979;18(3):296–7. https://doi.org/10.1021/i160071a019.
[70] Liu Z, Winterton RHS. A general correlation for saturated and subcooled flow boiling in tubes and annuli, based on a nucleate pool boiling equation. Int J Heat Mass Transf 1991;34(11):2759–66. https://doi.org/10.1016/0017-9310(91)90234-6.
[71] Friedel L. Improved friction pressure drop correlation for horizontal and vertical two-phase pipe flow. Eur Two-Phase Flow Group Meeting 1979:485–92.
[72] Cavallini A, et al. Condensation in horizontal smooth tubes: a new heat transfer model for heat exchanger design. Heat Transfer Eng 2006;27(8):31–8. https://doi.org/10.1080/01457630600793970.
[73] Castell A, Solé C, Medrano M, Roca J, Cabeza LF, García D. Natural convection heat transfer coefficients in phase change material (PCM) modules with external vertical fins. Appl Therm Eng 2008;28(13):1676–86. https://doi.org/10.1016/j.applthermaleng.2007.11.004.
[74] Medrano M, Yilmaz MO, Nogués M, Martorell I, Roca J, Cabeza LF. Experimental evaluation of commercial heat exchangers for use as PCM thermal storage systems. Appl Energy 2009;86(10):2047–55. https://doi.org/10.1016/j.apenergy.2009.01.014.
[75] Alfani D, Giostri A, Astolfi M. Working fluid selection and thermodynamic optimization of the novel renewable energy-based RESTORE seasonal storage technology. J Eng Gas Turbines Power 2024;146(10). https://doi.org/10.1115/1.4065407.
[76] Held TJ, et al. Compressor development for CO2-based pumped thermal energy storage Systems. J Eng Gas Turbines Power 2025;147(9). https://doi.org/10.1115/1.4067449.
[77] Guizzi GL, Manno M, Tolomei LM, Vitali RM. Thermodynamic analysis of a liquid air energy storage system. Energy 2015;93:1639–47. https://doi.org/10.1016/j.energy.2015.10.030.
[78] Hartmann N, Vöhringer O, Kruck C, Eltrop L. Simulation and analysis of different adiabatic compressed air energy storage plant configurations. Appl Energy 2012;93:541–8. https://doi.org/10.1016/j.apenergy.2011.12.007.